

Collective flow and hydrodynamics in large and small systems at the LHC

Huichao Song^{1,2,3} · You Zhou⁴ · Katarína Gajdošová⁴

Received: 24 December 2016 / Revised: 3 March 2017 / Accepted: 9 March 2017 / Published online: 6 June 2017

© Shanghai Institute of Applied Physics, Chinese Academy of Sciences, Chinese Nuclear Society, Science Press China and Springer Science+Business Media Singapore 2017

Abstract In this article, we briefly review the recent progress on collective flow and hydrodynamics in large and small systems at the Large Hadron Collider (LHC), which includes the following topics: extracting the QGP viscosity from the flow data, initial-state fluctuations and final-state correlations at 2.76 A TeV Pb–Pb collisions, correlations, and collective flow in high-energy p–Pb and p–p collisions.

Keywords Collective flow · Hydrodynamics · QGP

1 Introduction

At extremely high temperatures and densities, the strong-interaction matter can experience a phase transition and form a hot and thermalized medium called the quark–

gluon plasma (QGP), where quarks and gluons are no longer confined but propagate over larger distances than the typical size of a hadron [1, 2]. Around a few microseconds after the Big Bang, the QGP once filled in the whole early universe. With the expansion and cooling down of the universe, the primordial QGP went through a phase transition and formed hadrons, including protons and neutrons, the basic building blocks of our current visible world. The QGP can also be created at the Relativistic Heavy Ion Collider (RHIC) and the Large Hadron Collider (LHC), where the ultra-relativistic collisions of heavy ions allow us to achieve the needed extreme conditions for the QCD phase transitions and for the formation of the QGP [1–3].

Since the running of RHIC in 2000, strong evidence was gradually accumulated for the creation of the QGP in the high-energy nucleus–nucleus collisions [4–9]. The observation of strong collective flow and the successful descriptions from hydrodynamics reveal that the QGP is a strongly coupled system and behaves like an almost perfect liquid [8–10]. It was also realized that, since the nucleons inside the colliding nuclei constantly change their positions, the created QGP fireballs fluctuate event-by-event [11–13]. The collective expansion of the hot systems transforms the initial spacial inhomogeneities and deformation into anisotropic momentum distributions of final produced particles [14, 15], which can be quantitatively evaluated by various flow observables [16–22]. For example, the elliptic flow v_2 is associated with the elliptic deformation of the initial fireball, the triangular flow v_3 is mainly controlled by the event-by-event fluctuations of the systems and the quadrangular flow v_4 is driven by both initial spacial deformations and inhomogeneities of the created fireball, etc [23–26]. Besides these individual flow

This work was supported by the NSFC and the MOST (Nos.11435001, 11675004 and 2015CB856900) and the Danish Council for Independent Research, Natural Sciences, and the Danish National Research Foundation (Danmarks Grundforskningsfond).

✉ Huichao Song
Huichaosong@pku.edu.cn

You Zhou
you.zhou@cern.ch

¹ Department of Physics and State Key Laboratory of Nuclear Physics and Technology, Peking University, Beijing 100871, China

² Collaborative Innovation Center of Quantum Matter, Beijing 100871, China

³ Center for High Energy Physics, Peking University, Beijing 100871, China

⁴ Niels Bohr Institute, University of Copenhagen, Blegdamsvej 17, 2100 Copenhagen, Denmark

harmonics, other flow observables, such as v_n in ultra-central collisions [27, 28], the distributions of event-by-event flow harmonics [29, 30], the event-plane correlations [31, 32], and the correlations between different flow harmonics [33–37], the de-correlation of the flow vector [38–40], have also been intensively measured and studied in the high-energy Pb–Pb collisions at the LHC. Together with the sophisticated event-by-event simulations from hydrodynamics and hybrid models, these different flow observables provide important information on the properties of the QGP fireball and help to constrain the initial conditions of the colliding systems [16–22].

The measurements of the azimuthal correlations in small systems, e.g., in p–Pb and p–p collisions at the LHC, were originally aimed to provide the reference data for the high-energy nucleus–nucleus collisions. However, lots of unexpected phenomena were discovered in experiments, which indicate the development of collective flow in the small systems. As the collision energy increased to the LHC regime, the multiplicities in “ultra-central” p–Pb and p–p collisions is comparable to the ones in peripheral Pb–Pb collisions, where that final-state interactions become possibly sufficient to develop the collective expansion. A comparison of the two-particle correlations in high-multiplicity p–Pb collisions at $\sqrt{s_{NN}} = 5.02$ TeV and in peripheral Pb–Pb collisions at $\sqrt{s_{NN}} = 2.76$ TeV shows a surprisingly similar correlation structure for these events with similar multiplicity cuts [41–44]. Besides, a changing sign of the 4-particle cumulants [43–45] and a v_2 mass mass-ordering feature of identified hadrons [46, 47] and other flow-like signals have also been observed in the high-multiplicity p–Pb collisions. The related hydrodynamic simulations have successfully reproduced many of this experimental data, which strongly support the observation of collective flow in high-multiplicity p–Pb collisions [48–54]. For p–p collisions at $\sqrt{s_{NN}} = 7$ and 13 TeV, similar results, but with smaller magnitudes, have been obtained for many of these flow-like observables [55–60]. Although these measurements may be associated with the collective expansion in the small p–p systems, more detailed investigations are still needed to further understand the physics behind them.

In this paper, we will review the recent progress on collective flow and hydrodynamics in large and small systems at the LHC. In Sects. 2 and 3, we will introduce hydrodynamics, hybrid models, and flow measurements. In Sect. 4, we will review recent progress on extracting the QGP viscosity from the flow data at the LHC. In Sect. 5, we will focus on initial-state fluctuations and final-state correlates in Pb–Pb collisions at 2.76 A TeV. In Sect. 6, we will review the correlations and collective flow in small

systems. Section 7 will briefly summarize and conclude this paper.

2 Hydrodynamics and hybrid model

2.1 Viscous hydrodynamics

Viscous hydrodynamics are a widely used tool to describe the expansion of the QGP fireball and to study the soft hadron data for the heavy ion collisions at RHIC and the LHC [18–20, 61–73]. It solves the transport equations of energy-momentum tensor and net charge current, which are written as

$$\partial_\mu T^{\mu\nu}(x) = 0, \tag{1a}$$

$$\partial_\mu N^\mu(x) = 0. \tag{1b}$$

If the systems are very close to local equilibrium, the energy-momentum tensor and the net baryon charge current can be decomposed as: $T^{\mu\nu} = (e + p)u^\mu u^\nu - pg^{\mu\nu}$ and $N^\mu = nu^\mu$. Therefore, the fourteen variables in $T^{\mu\nu}$ and N^μ are reduced to six independent unknowns: the energy density, e , pressure, p , and net baryon density, n , and 3 independent components in the four velocity, u^μ . The relativistic hydrodynamics are then simplified as ideal hydrodynamics. With an additional input, the equation of state (EoS), $p = p(n, e)$, and the chosen initial and final conditions, the ideal hydrodynamic equations can be numerically solved to simulate the evolution of the bulk matter for the relativistic heavy ion collisions [10].

For a near equilibrium system, one needs to implement the relativistic viscous hydrodynamics (or the so-called relativistic dissipative fluid dynamics). In the Landau frame, $T^{\mu\nu}$ and N^μ are expressed as: $T^{\mu\nu} = (e + p + \Pi)u^\mu u^\nu - (p + \Pi)g^{\mu\nu} + \pi^{\mu\nu}$, $N^\mu = nu^\mu - \frac{n}{e+p}q^\mu$. Here, $\pi^{\mu\nu}$ is the shear stress tensor, Π is the bulk pressure, and q^μ is the heat flow. From the 2nd law of thermal dynamics or from the kinetic theory, one could obtain the viscous equations of $\pi^{\mu\nu}$, Π , and q^μ , which are expressed as [74, 75]:

$$\Delta^{\mu\alpha}\Delta^{\nu\beta}\dot{\pi}_{\alpha\beta} = -\frac{1}{\tau_\pi}\left[\pi^{\mu\nu} - 2\eta\nabla^{\langle\mu}u^{\nu\rangle} - l_{\pi q}\nabla^{\langle\mu}q^{\nu\rangle} + \pi_{\mu\nu}\eta T\partial_\alpha\left(\frac{\tau_\pi u^\alpha}{2\eta T}\right)\right], \tag{2a}$$

$$\dot{\Pi} = -\frac{1}{\tau_\Pi}\left[\Pi + \zeta\theta - l_{\Pi q}\nabla_\mu q^\mu + \Pi\zeta T\partial_\mu\left(\frac{\tau_\Pi u^\mu}{2\zeta T}\right)\right], \tag{2b}$$

$$\Delta_v^\mu q^v = -\frac{1}{\tau_q} \left[q_\mu + \lambda \frac{nT^2}{e+p} \nabla^\mu \frac{v}{T} + l_{q\pi} \nabla_\nu \pi^{\mu\nu} + l_{q\Pi} \nabla^\mu \Pi - \lambda T^2 q^\mu \partial_\mu \left(\frac{\tau_q u^\mu}{2\lambda T^2} \right) \right], \quad (2c)$$

where $\Delta^{\mu\nu} = g^{\mu\nu} - u^\mu u^\nu$, $\nabla^{\langle\mu} u^{\nu\rangle} = \frac{1}{2}(\nabla^\mu u^\nu + \nabla^\nu u^\mu) - \frac{1}{3}\Delta^{\mu\nu} \partial_\alpha u^\alpha$, and $\theta = \partial \cdot u$. η is the shear viscosity, ζ is the bulk viscosity, λ is the heat conductivity, and τ_π , τ_Π , and τ_q are the corresponding relaxation times.

The above Israel–Stewart formalism can also be obtained from the kinetic theory [76–80] or from the conformal symmetry constraints [77].¹ These different derivations give different higher-order terms for the second-order viscous equations. In general, the contributions of the higher-order terms are pretty small or even negligible for a hydrodynamic evolution with small shear and bulk viscosity, which will not significantly influence the final flow observables.²

2.1.1 The equations of state (EoS)

Besides these hydrodynamic equations, one needs to input an EoS to close the system for the numerical simulations or analytical solutions. Currently, many groups use a state-of-the-art EoS, called s95p-PCE, which combines a parameterized/tabulated lattice EoS for the baryon free QGP phase with a hadronic EoS with effective chemical potentials for the partially chemical equilibrium hadronic phase [100, 101]. Reference [100] also compared the hydrodynamic calculations using various equations of state constructed with a different speed of sound, which found that the spectra and elliptic flow are only slightly influenced by the inputting EoS. The main uncertainties of the hydrodynamic calculations come from the initial conditions, which will be introduced and discussed below.

2.1.2 Initial conditions

The initial condition is a necessary input for the hydrodynamic simulations. As an open issue related to the creation and thermalization of the QGP, it brings some

uncertainties, more or less, for many flow observables in the hydrodynamic calculations. There are many types of initial condition models developed by different groups. The traditional Glauber model assumes zero transverse velocity at the starting time and constructs the initial entropy/energy density profiles from a mixture of the wounded nucleon and binary collision densities [102]. The KLN model treats the degrees of freedom of the initial systems as gluons and calculates the initial density profiles from the k_T factorization formula [103]. In the later developed Monte Carlo versions, called (MC-Glauber and MC-KLN) [104–106], the event-by-event fluctuations are built through the positions fluctuations of individual nucleons inside each colliding nuclei. For the AMPT initial conditions, the initial profiles are constructed from the energy and momentum decompositions of individual partons, which fluctuate in both momentum and position space [107–109]. With an additional Gaussian smearing factor, the fluctuation scales related to the energy decompositions become changeable, which helps to balance the initial eccentricities at different order. As a successful initial condition model, IP-Glasma [110] includes both the nucleon position fluctuations and the color charge fluctuations. It uses the IP-Sat model to generate the wavefunctions of high-energy nuclei/nucleon and then implements a classical Yang-Mills dynamic to simulate the pre-equilibrium evolution of the early glasma stage. Another successful initial condition model in EKRT [111, 112] combines the PQCD minijet production with the gluon saturation and generates the energy density profiles after a pre-equilibrium Bjorken free streaming. The recently developed T_RENTO model [113] is a parametric initial condition model based on the eikonal entropy deposition via a reduced thickness function. With an introduced entropy deposition parameter, the T_RENTO model could reproduce the initial eccentricities of various initial condition models that belong to different classes, such as MC-KLN, MC-Glauber, EKRT, IP-Glasma.

Many initial condition models neglect the initial flow from the pre-equilibrium stage. Recently, the effects of pre-equilibrium evolution have been estimated in Ref. [114] through evolving the free-streaming particles from MC-Glauber and MC-KLN models, which demonstrated that such pre-equilibrium dynamics significantly increase the initial flow and reduce the initial spacial eccentricities. More sophisticated investigations on pre-equilibrium dynamics can be, in principle, carried on within the framework of dynamical models like EPOS [115], AMPT [107–109], EKRT [111, 112], IP-Glasma [110], URQMD [116, 117]. After matching the energy-momentum tensor at a switching point, one could principally obtain 3+1-d fluctuating profiles of initial energy density and initial flow for the succeeding hydrodynamic simulations. However,

¹ The traditional second-order viscous hydrodynamics works for a near equilibrium system with isotropic momentum distributions. It cannot apply to an anisotropic system at very early time [81–83] or a correlated fluctuating system near the QCD critical point [84–87] where the traditional expansion of the microscopic distribution function fails. For the recent development on anisotropic hydrodynamics or chiral hydrodynamics, please refer to [81–83, 88–93] and [94–98].

² Note that, to obtain a good agreement with the microscopic kinetic theory, a proper resummation of the irreducible moments is essential for the computation of the transport coefficients, especially for a fluid dynamics with heat flow included. Please refer to [99] for details.

many past studies focus on the initial-state fluctuations on the transverse plane, which neglect the fluctuation patterns along the longitudinal direction. The AMPT + ideal hydrodynamic simulations [108] demonstrate that evolving early hot spots in the longitudinal directions could dissipate part of the transverse energy, which leads to a suppression of the final flow anisotropy. Recently, the IP-Glasma model has been extended to three dimension with the explicit small x evolutions of the gluon distributions [118]. Although the related energy-momentum tensors can be, in principle, used in the succeeding hydrodynamic simulations, additional works are still required to further extend the distributions to the large rapidity regime with the consideration of large x effects.

2.1.3 Freeze-out/decoupling

Pure hydrodynamic simulations assume free-streaming hadrons directly emitted from a decoupling surface defined by a constant temperature, energy density, or other kinetic variables [10, 61]. The momentum distributions of various emitted thermal hadrons can be calculated with the Cooper–Frye formula [119] using the freeze-out information on the freeze-out surface (For the details of the Cooper–Frye formula, please refer to [10, 119] as well as the following Sect. 2.2 for details). With the corresponding decay channels, the unstable hadron resonances delay into stable ones with some momentum distributions that can be further analyzed and compared with the experimental data. In the constant temperature decoupling scenario, the decoupling temperature, T_{dec} strongly depends on the EoS and other hydrodynamic inputs. For s95p-PCE, T_{dec} is generally set to 100–120 MeV in order to fit the mean pT of various hadrons with a sufficient build up of the radial flow [10, 101].

2.2 Hybrid models

A hybrid model matches the hydrodynamic description of the QGP fluid to a hadron cascade simulation for the evolution of the hadron resonance gas at a switching temperature near T_c . The early ideal hydrodynamics + hadron cascade hybrid model simulations have showed that the hadronic matter is highly viscous, which largely suppress the elliptic flow when compared with the pure hydrodynamic calculations with a partially chemical equilibrium EoS [120]. Motivated by this, different groups have extended 2+1-d or 3+1-d viscous hydrodynamic simulations with a hadronic afterburner [121–123]. Such hybrid models give a more realistic description for the hadronic evolution of the QGP fireball, which also

naturally imprint the off-equilibrium chemical and thermal freeze-out procedures of various hadron species.

The key component of a hybrid model is the particle event generator that converts the hydrodynamic output on the switching hyper surface into various hadrons for the succeeding hadron cascade simulations. More specifically, such Monte Carlo event generators produce particles with specific momentum and position information according to the differential Cooper–Frye formula [121]:

$$E \frac{d^3 N_i}{d^3 p}(x) = \frac{g_i}{(2\pi)^3} p \times d^3 \sigma(x) f_i(x, p), \quad (3)$$

where $f_i(x, p)$ is the distribution function of hadron species, i , g_i is the corresponding degeneracy factor, and $d^3 \sigma_\mu(x)$ is a surface element on the hyper surface, Σ , e.g., defined by a constant switching temperature T_{sw} . Generally, the switching temperature, T_{sw} , is set to around 160 MeV, which is close to the phase transition temperature of the QCD matter at zero chemical potential [124]. For a viscous QGP fluid, the distribution function $f(x, p)$ includes an ideal part and an off-equilibrium part $f = f_0 + \delta f$, where δf generally takes the form: $\delta f = f_0 (1 \mp f_0) \frac{p^\mu p^\nu \pi_{\mu\nu}}{2T^2(e+p)}$ [64–69]³.

After converting the fluid into many individual hadrons of various species, the hybrid model implements a hadron cascade model to simulate the microscopic evolution of the hadron resonance gas. The hadron cascade model, for example, the Ultra-relativistic Quantum Molecular Dynamics (UrQMD) [127, 128] solves a large set of Boltzmann equations for various hadron species:

$$\frac{df_i(x, p)}{dt} = C_i(x, p), \quad (4)$$

where $f_i(x, p)$ is the distribution function and $C_i(x, p)$ is the collision terms for the hadron species, i . With such equations, the hadron cascade model propagates various hadrons with classical trajectories, together with the elastic scatterings, inelastic scatterings, and resonance decays. After all the collisions and decays cease, the system stops evolution and outputs the information of the produced hadron, which can be further analyzed to be compared with the corresponding experimental data [127, 128].

³ The full off-equilibrium distribution includes the contributions from shear stress tensor, bulk pressure and heat flow: $\delta f = \delta f_{shear} + \delta f_{bulk} + \delta f_{heat}$. For the bulk viscous correction, there are different proposed forms of δf_{bulk} [125, 126], which brings certain amount of uncertainties for some related flow observables. Considering this complicity as well as the negligible heat conductivity, one generally takes this simple form of δf with only shear viscous correction for the viscous hydrodynamics and hybrid model calculations at top RHIC and the LHC energies.

Compared with the early hydrodynamic calculations, the hybrid model improves the description of the hadronic evolutions and the decoupling procedure, which leads to a nice description of the flow harmonics of identified hadrons, especially for the mass splitting between pions and protons [129, 130]. Meanwhile, the imprinted baryon–antibaryon ($B - \bar{B}$) annihilations in the hadronic cascade sector also largely reduce the production of proton and antiproton, which helps to achieve a nice fit of particle yields of various hadron species [129, 131].

2.2.1 2+1-d vs 3+1-d model

For hydrodynamics or hybrid models, the 2+1-d simulations with a longitudinal boost invariance are more computationally efficient than the full 3+1-d simulations. Before 2010, many developed viscous hydrodynamic codes are (2+1)-dimensional using the Bjorken approximation [64–72]. The published VISHNU code is also basically a (2+1)-d hybrid code since it implements the (2+1)-d viscous hydrodynamic simulations for the evolution of the QGP phase. Although the succeeding UrQMD afterburner are (3+1)-dimensional, the longitudinal boost invariance is still approximately conserved at mid-rapidity after the hadronic evolution [121]. Recently, several groups [73, 132–136] further developed the full (3+1)-d viscous hydrodynamics or hybrid models without a longitudinal boost invariance. Such full (3+1)-d simulations could provide full space-time evolution profiles for the EM and hard probes. They can also be widely used to investigate the longitudinal fluctuations, to study the physics for asymmetric collision systems, such as p+Pb, d+Au, and Cu+Au, and to provide more realistic calculations / predictions for the heavy ion collisions at lower collision energies.

2.3 Event-by-event simulations

As introduced in Sect. II A, the initial profiles of the created QGP fireball fluctuate event-by-event, which leads to the final-state correlations and collective flow for the nucleus–nucleus collisions at RHIC and the LHC [11–13]. For computational efficiency, the early hydrodynamics or hybrid model simulations input smooth initial profiles obtained through averaging a large number of events generated from some specific fluctuating initial conditions and then implement the so-called *single-shot simulations*. An alternative approach is the *event-by-event simulations*, which simultaneously run a large number of simulations with the input of individually fluctuating initial profiles. Past research has shown, due to the approximate linear hydrodynamic response $v_2 \propto \varepsilon_2$ and $v_3 \propto \varepsilon_3$, the elliptic

and triangular flow can be nicely described by the single-shot hydrodynamic simulations with properly chosen initial conditions and well-tuned parameter sets. However, the single-shot simulation fails to describe other higher-order flow harmonics due to the mode coupling effects. Furthermore, some flow observables, such as event-by-event flow harmonics [29, 30], the event-plane correlations [31, 32], and the correlations between different flow harmonics [33–37], cannot be directly calculated by the single-shot hydrodynamics or hybrid models, which are required to implement the event-by-event simulations (please also refer to Sect. 5 for details).

Since 2010, many groups have developed event-by-event hydrodynamics / hybrid models to study the initial fluctuations, hydrodynamic response, and the corresponding final-state correlations [30, 32, 107–112, 137–141]. In general, such event-by-event simulations are computationally expensive. For example, the iEBE-VISHNU simulations for the correlations between flow harmonics have used 30,000 CPU hours in the Tianhe-1A National Supercomputing Center in Tianjin, China. Recently, the OSU-Kent group has developed the massively parallel simulations for 3+1-d viscous hydrodynamics on graphics processing units with CUDA and demonstrated that such GPU simulations are approximately two orders of magnitude faster than the corresponding simulations from CPU [142]. With the development of computer science and the reduced cost of GPU, the GPU-based simulations will become a popular trend for the massive hydrodynamic calculations in the future.

3 Flow method

The anisotropic flow evaluates the anisotropy in particle momentum distributions correlated with the flow symmetry plane, Ψ_n [14]. The various characteristic patterns of the anisotropic flow can be obtained from a Fourier expansion of the event averaged azimuthal particle distribution [15]:

$$\frac{dN}{d\varphi} \propto 1 + 2 \sum_{n=1}^{\infty} v_n e^{in(\varphi - \Psi_n)}, \quad (5)$$

where $v_n = \langle \cos n(\varphi - \Psi_n) \rangle$ is anisotropic flow and Ψ_n is the corresponding flow symmetry plane.

Since the flow symmetry plane is not a direct observable, the anisotropic flow, v_n , cannot be measured directly. A popular approach is the event-plane method [143], which has been widely used to calculate the azimuthal correlation of emitted particles with respect to the event plane. However, it was found that the results from the event-plane method strongly depend on the resolution of

the event plane, which introduces an uncontrolled bias in the measurement [144]. As an alternative approach, the multi-particle azimuthal correlations method [145, 146] has been developed and improved in the past ten years, which allows an unambiguous measurement of the underlying anisotropic flow and eliminates the detector bias.

3.1 2- and multi-particle correlations

Azimuthal correlations of 2 or multi-particles are calculated in two steps [145, 146]. First, one obtains an average over all particles in a single event and then calculates an average over all events. The single-event 2-particle correlation is defined as:

$$\langle \cos n(\varphi_1 - \varphi_2) \rangle = \langle e^{in(\varphi_1 - \varphi_2)} \rangle. \tag{6}$$

Here, $\langle \dots \rangle$ denotes an average over all particles in a single event. An average of the 2-particle correlation over all events is generally denoted by $\langle\langle \dots \rangle\rangle = \langle\langle e^{in(\varphi_1 - \varphi_2)} \rangle\rangle$. Such correlations can serve as an estimate of the flow harmonics, v_n , without the knowledge of the symmetry plane, which can also be demonstrated as:

$$\begin{aligned} \langle\langle e^{in(\varphi_1 - \varphi_2)} \rangle\rangle &= \langle\langle e^{in(\varphi_1 - \Psi_n - \varphi_2 + \Psi_n)} \rangle\rangle \\ &= \langle\langle e^{in(\varphi_1 - \Psi_n)} \rangle\rangle \langle\langle e^{in(\varphi_2 - \Psi_n)} \rangle\rangle + \delta_n \approx \langle v_n^2 \rangle + \delta_n, \end{aligned} \tag{7}$$

where δ_n is called non-flow. It is a term related to the statistical fluctuations, which implies that $\langle AB \rangle \neq \langle A \rangle \langle B \rangle$, or originated from the 2-particle correlations that is not associated with the collective expansion [17].

The formulas above can be extended to a generic notation for the average single-event k-particle correlators with mixed harmonics:

$$\langle \cos(n_1\varphi_1 + n_2\varphi_2 + \dots + n_i\varphi_i) \rangle (n_1 \geq n_2 \geq \dots \geq n_i). \tag{8}$$

Here, the azimuthal angle, φ_i , belongs to the reconstructed particle, i . The self-correlations should be removed completely with only genuine multi-particle correlations left. For simplicity, we also denote these k -particle correlators as $\langle k \rangle_{n_1, n_2, \dots, n_k}$ in the following context. As the case for the 2-particle correlator, the subsequent average over all events can be obtained in a similar way described in Eq. (7). For details, please refer to [147].

Calculations for the single event averaged multi-particle correlators require a large amount of computational resources, which significantly increase for higher-order correlations. A successful way to calculate these correlators is in a single loop over particles in one event and can be achieved by the Q-vectors, which will be introduced in the following text.

3.1.1 Q-cumulant method

In the Q-cumulant method [145], the single-event averaged correlations are calculated in terms of a Q_n -vector, which is defined as:

$$Q_n \equiv \sum_{i=1}^M e^{in\phi_i}, \tag{9}$$

where M is the number of particles in a specific event, and ϕ_i is the azimuthal angle of the i -th particle. For azimuthal correlations involving only a single harmonic, the single-event average 2-, and the 4-particle azimuthal correlations can be calculated as:

$$\langle 2 \rangle_{n,-n} = \frac{|Q_n|^2 - M}{M(M-1)}, \tag{10}$$

$$\begin{aligned} \langle 4 \rangle_{n,n,-n,-n} &= [|Q_n|^4 + |Q_{2n}|^2 - 2 \cdot \text{Re}(Q_{2n} Q_n^* Q_n^*) \\ &\quad - 2[2(M-2) \cdot |Q_n|^2 - M(M-3)]] \\ &\quad / [M(M-1)(M-2)(M-3)]. \end{aligned} \tag{11}$$

After averaging the correlators over the whole event sample, one obtains the 2- and 4-particle cumulants:

$$c_n\{2\} = \langle\langle 2 \rangle\rangle_{n,-n} \tag{12}$$

$$c_n\{4\} = \langle\langle 4 \rangle\rangle_{n,n,-n,-n} - 2 \langle\langle 2 \rangle\rangle_{n,-n}^2. \tag{13}$$

Eventually, the 2- and 4-particle and reference (integrated) flow harmonics can be calculated as:

$$v_n\{2\} = \sqrt{c_n\{2\}}, \quad v_n\{4\} = \sqrt[4]{-c_n\{4\}}. \tag{14}$$

The differential flow harmonics for identified or all charged hadrons can be obtained from a single-event correlators averaged over only these particles of interest within an event. For the limitation of space, we will not further outline the lengthy formula, but refer to [145] for details.

As pointed out above, the non-flow effects, originated from resonance decays, jets, etc., could strongly influence the calculated flow harmonics, especially for the ones obtained from 2-particle correlations. In order to largely suppress the non-flow contribution, a successful method of applying a $|\Delta\eta|$ gap to 2-particle correlations has been developed. In this method, an analyzed event is divided into 2 sub-events with certain $|\Delta\eta|$ separation. After obtaining the Q-vectors for each sub-event separately, the single-event average 2-particle correlation with $|\Delta\eta|$ gap can be calculated as:

$$\langle 2 \rangle_{n,-n}^{|\Delta\eta|} = \frac{Q_n^A \times Q_n^{B*}}{M^A \times M^B}, \tag{15}$$

where A and B denote two different sub-events. The corresponding final flow harmonics are usually denoted as:

$v_n\{2, |\Delta\eta| > X\}$, which can be obtained in the same way as the above reference flow without the $|\Delta\eta|$ gap.

3.1.2 Generic framework

In 2013, a generic framework was developed [146] which enables exact and efficient evaluation of all multi-particle azimuthal correlations. This framework can be used along with a correction framework for systematic biases in anisotropic flow analyses due to the Non-Uniform Acceptance (NUA) and Non-Uniform Efficiency (NUE) effects. For an event with multiplicity, M , it was proposed to construct two sets for azimuthal angles of the particles $\{\varphi_1, \varphi_2, \dots, \varphi_M\}$ and for the corresponding weights $\{w_1, w_2, \dots, w_M\}$. With these two sets, one can calculate the weighted Q_n -vectors in each event, which is defined as:

$$Q_{n,p} \equiv \sum_{i=1}^M w_i^p e^{in\varphi_i}, \quad (16)$$

where w_i is the weight and p is the power of the weight. Correspondingly, the i -particle correlator is defined as:

$$N\langle m \rangle_{n_1, n_2, \dots, n_m} \equiv \sum_{\substack{i_1, i_2, \dots, i_m=1 \\ i_1 \neq i_2 \neq \dots \neq i_m}}^M w_{i_1} w_{i_2} \dots w_{i_m} e^{i(n_1\varphi_{i_1} + n_2\varphi_{i_2} + \dots + n_m\varphi_{i_m})} \quad (17)$$

Here, the i -particle correlator is denoted as $N\langle m \rangle_{n_1, n_2, \dots, n_m}$ for convenience. One could also introduce a shortcut $D\langle m \rangle_{n_1, n_2, \dots, n_m} = N\langle m \rangle_{0, 0, \dots, 0}$ and then calculate the single-event average of multi-particle azimuthal correlations via:

$$\langle m \rangle_{n_1, n_2, \dots, n_m} = \frac{N\langle m \rangle_{n_1, n_2, \dots, n_m}}{D\langle m \rangle_{n_1, n_2, \dots, n_m}}. \quad (18)$$

Based on this generic framework, one could explicitly outline the results for the 2- and 4-particle correlators, which can be analytically expressed in terms of the $Q_{n,p}$ -vectors defined in the above context. The single-event average at 2- and 4-particle correlations could then be calculated as:

$$\langle 2 \rangle_{n_1, n_2} = \frac{N\langle 2 \rangle_{n_1, n_2}}{D\langle 2 \rangle_{n_1, n_2}}, \quad (19)$$

$$\langle 4 \rangle_{n_1, n_2, n_3, n_4} = \frac{N\langle 4 \rangle_{n_1, n_2, n_3, n_4}}{D\langle 4 \rangle_{n_1, n_2, n_3, n_4}}. \quad (20)$$

Here $N\langle 2 \rangle_{n_1, n_2}$ and $D\langle 2 \rangle_{n_1, n_2}$ could be obtained as:

$$N\langle 2 \rangle_{n_1, n_2} = Q_{n_1, 1} Q_{n_2, 1} - Q_{n_1+n_2, 2} \quad (21)$$

$$D\langle 2 \rangle_{n_1, n_2} = N\langle 2 \rangle_{0, 0} = Q_{0, 1}^2 - Q_{0, 2}. \quad (22)$$

Similarly, one can calculate $N\langle 4 \rangle_{n_1, n_2, n_3, n_4}$ and $D\langle 4 \rangle_{n_1, n_2, n_3, n_4}$ as follows:

$$\begin{aligned} N\langle 4 \rangle_{n_1, n_2, n_3, n_4} = & Q_{n_1, 1} Q_{n_2, 1} Q_{n_3, 1} Q_{n_4, 1} - Q_{n_1+n_2, 2} Q_{n_3, 1} Q_{n_4, 1} \\ & - Q_{n_2, 1} Q_{n_1+n_3, 2} Q_{n_4, 1} - Q_{n_1, 1} Q_{n_2+n_3, 2} Q_{n_4, 1} \\ & + 2Q_{n_1+n_2+n_3, 3} Q_{n_4, 1} - Q_{n_2, 1} Q_{n_3, 1} Q_{n_1+n_4, 2} \\ & + Q_{n_2+n_3, 2} Q_{n_1+n_4, 2} - Q_{n_1, 1} Q_{n_3, 1} Q_{n_2+n_4, 2} \\ & + Q_{n_1+n_3, 2} Q_{n_2+n_4, 2} + 2Q_{n_3, 1} Q_{n_1+n_2+n_4, 3} \\ & - Q_{n_1, 1} Q_{n_2, 1} Q_{n_3+n_4, 2} + Q_{n_1+n_2, 2} Q_{n_3+n_4, 2} \\ & + 2Q_{n_2, 1} Q_{n_1+n_3+n_4, 3} + 2Q_{n_1, 1} Q_{n_2+n_3+n_4, 3} \\ & - 6Q_{n_1+n_2+n_3+n_4, 4}, \end{aligned} \quad (23)$$

$$\begin{aligned} D\langle 4 \rangle_{n_1, n_2, n_3, n_4} = N\langle 4 \rangle_{0, 0, 0, 0} \\ = Q_{0, 1}^4 - 6Q_{0, 1}^2 Q_{0, 2} + 3Q_{0, 2}^2 \\ + 8Q_{0, 1} Q_{0, 3} - 6Q_{0, 4}. \end{aligned} \quad (24)$$

The analogous results for higher-order correlators and differential flow can be written out in a similar manner. The details can be found in [146].

Last but not least, the generic framework not only corrects the NUA and NUE effects exactly and efficiently, it can also be applied in any order of multi-particle correlations for the cases where their direct implementation was not feasible before. For instance, Eqs. (19) and (20) could be used in Symmetric cumulants $SC(4, 2)$ (discussed in Sect.V) by calculating the 4-particle correlation of $\langle 4 \rangle_{4, 2, -4, -2}$, and the 2-particle correlations $\langle 2 \rangle_{2, -2}$ and $\langle 2 \rangle_{4, -4}$.

4 Extracting the QGP viscosity from flow harmonics

4.1 Semi-quantitative extractions of the QGP shear viscosity

The hydrodynamic calculations from different groups have shown that the flow harmonics are sensitive to the QGP shear viscosity, η/s , which can be used to study the transport properties of the hot QCD matter [18–20, 61–73]. Around 2008, the INT group made an early extraction of the QGP shear viscosity from the integrated and differential elliptic flow data in 200 A GeV Au–Au collisions using the 2+1-d viscous simulations with optical Glauber and KLN initializations [64, 65]. They found these two initial conditions bring large uncertainties for the extracted value of η/s around O (100%). However, it is not reliable to directly read the value of η/s from the direct model to the data comparison since their model calculations neglect the

high viscous and even off-equilibrium hadronic evolution, which only treat such stages as a pure viscous fluid expansion with both chemical and thermal equilibrium. Reference [65, 152] further estimated the effects from the late hadronic evolution and concluded that the extracted value of the specific QGP shear viscosity $(\eta/s)_{QGP}$, cannot exceed an upper limit of around $5 \times \frac{1}{4\pi}$.

For a realistic description of the evolution and decoupling of the hadronic matter, the OSU-LBL group further developed the VISHNU hybrid model [121] which combines the 2+1-d viscous hydrodynamics with a hadron cascade model-UrQMD and then made a semi-qualitative extraction of the QGP shear viscosity from the integrated elliptic flow data in 200 A GeV Au–Au collisions [148, 153]. Figure 1 shows the eccentricity-scaled integrated elliptic flow calculated from VISHNU with MC-Glauber and MC-KLN initial conditions together with a comparison with the corrected experimental data with the non-flow and fluctuation effects removed [149]. From Fig. 1, one finds $\frac{1}{4\pi} < (\eta/s)_{QGP} < 2.5 \times \frac{1}{4\pi}$, where the main uncertainties of the extracted $(\eta/s)_{QGP}$ still come from the undetermined initial conditions. Meanwhile, the corresponding VISHNU simulations with both MC-Glauber and MC-KLN initial conditions could nicely describe the pT -spectra and differential elliptic flow harmonics, $v_2(pT)$, for all charged and identified hadrons at various centrality bins in 200 A GeV Au–Au collisions [153]. Compared with the early extractions in Ref. [64], the precision of the extracted value of $(\eta/s)_{QGP}$ is largely increased due to a better description of the highly viscous hadronic stage.

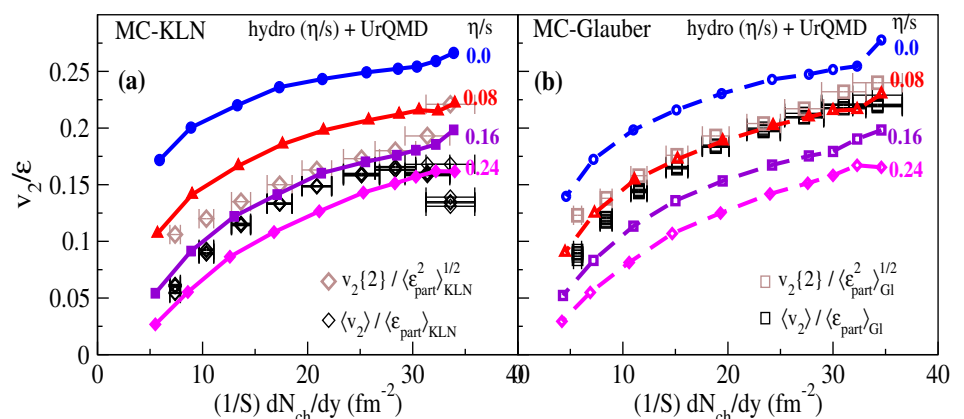
In Ref. [154], the VISHNU simulations were further extrapolated to the LHC energies, which systematically investigated the soft hadron data in the 2.76 A TeV Pb–Pb collisions. The related calculations have shown that with the same $(\eta/s)_{QGP}$ extracted at top RHIC energies, VISHNU slightly over-predicts the ALICE flow data at the LHC. After slightly increasing $(\eta/s)_{QGP}$ (for the MC-KLN initial conditions, $(\eta/s)_{QGP}$ increases from ~ 0.16

to ~ 0.20), VISHNU achieves a better description of the elliptic flow of all charged hadrons at various centralities [154].

Many of the early hydrodynamic or hybrid model simulations (includes these 2+1-d hydrodynamic and VISHNU calculations mentioned above) [121, 129, 130, 148, 153–155] belong to the category of single-shot simulations, which input smooth initial energy/entropy profiles from early initial condition models or input some smoothed profiles obtained from averaging millions of events from some specific fluctuating initial condition models. Correspondingly, the effects from initial-state fluctuations are neglected. Around 2012, the McGill group further developed event-by-event 3+1-d viscous hydrodynamic simulations with the IP-Glasma pre-equilibrium dynamics (MUSIC + IP-Glasma) and calculated the flow harmonics at different orders at the RHIC and the LHC [30]. Figure 2 shows the integrated and differential $v_n(n = 2, \dots, 5)$ of all charged hadrons in the 2.76 A TeV Pb–Pb collisions. Impressively, these different flow harmonics data are nicely described by the MUSIC simulations with $\eta/s = 0.2$ or a temperature dependent $\eta/s(T)$ at various centralities. Meanwhile, their simulations also show the averaged QGP viscosity is slightly larger at the LHC than at the RHIC, as found in Ref. [154]. Compared with the VISHNU simulations [148, 153, 154], these MUSIC calculations are purely hydrodynamic, which does not specially treat the hadronic evolution with a hadronic afterburner. However, the main results will not be significantly changed since the flow harmonics at the LHC energies are mainly developed (or even reach saturation) in the QGP phase.

For the hydrodynamic simulation with IP-Glasma initial conditions, a balanced initial eccentricities at different orders are generated at the beginning, which helps to achieve a simultaneous fit of the elliptic flow, triangular flow, and other higher-order harmonics. In contrast, the hydrodynamic calculations with either Mc-Glauber or Mc-

Fig. 1 (Color online) Eccentricity-scaled elliptic flow as a function of final multiplicity per area. The theoretical results are calculated from the VISHNU hybrid model calculations with MC-Glauber (left) and MC-KLN (right) initial conditions [148]. The experimental data are taken from Ref. [149]



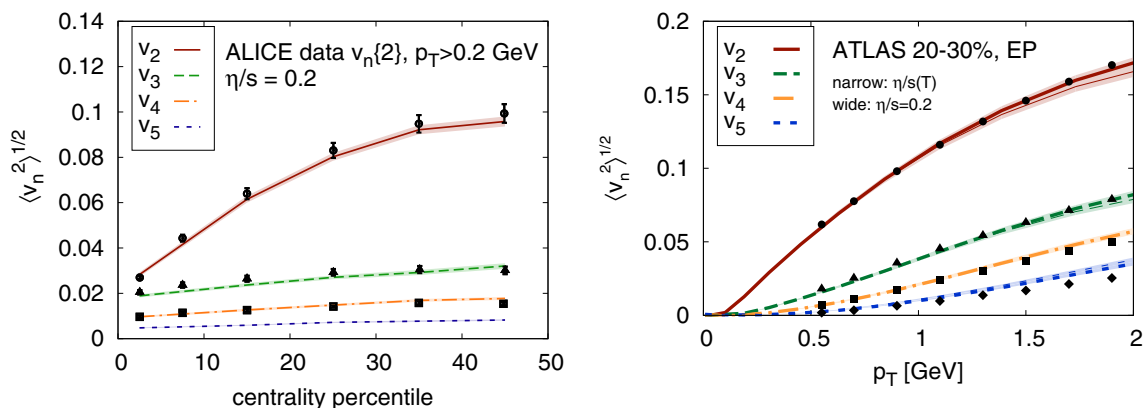


Fig. 2 (Color online) Root-mean-square anisotropic flow coefficients $\langle v_n^2 \rangle^{1/2}$ and $v_n(pT)$ in the 2.76 A TeV Pb–Pb collisions. The theoretical curves are calculated from MUSIC with IP-Glasma initial

conditions [30]. The experimental data in the *left* and *right* panels are measured by the ALICE collaboration [24] and the ATLAS collaboration, respectively

KLN initial conditions fail to simultaneously describe all the flow harmonics, v_n , at different orders ($n = 2 \dots 5$), although they can nicely fit the elliptic flow data with a well-tuned QGP shear viscosity. Therefore, these higher-order flow harmonic measurements disfavor these two initial conditions, which also motivated the later developments of other initial condition models. In short, the extracted value of the QGP viscosity may be largely influenced by the initial conditions used in the hydrodynamic calculations. Meanwhile, higher-order flow harmonics as well as other flow observables (please also refer to Sect. 5 for details) could put straight constraints for the initial condition models and for the extracted value of the QGP shear viscosity.

Besides the flow data of all charged hadrons, the flow harmonics of identified hadrons could reveal more information on the hadronic evolution of the hot QCD matter and provide additional tests for extracted values of the QGP transport coefficients obtained from the soft hadron data of all charged hadrons. References [129] and [130] have shown, for the extracted constant QGP shear viscosity obtained from the elliptic flow in 2.76 A TeV Pb–Pb collisions, the VISHNU hybrid model could nicely describe the differential elliptic flow data of pions, kaons, and protons [129, 130]. Meanwhile, it could also roughly fit the elliptic flow data of strange and multi-strange hadrons (Λ , Ξ , and Ω) measured at the LHC [155]. Recently, the ALICE collaboration further measured the higher-order flow harmonics of identified hadrons in the 2.76 A TeV Pb–Pb collisions, which showed that the triangular and quadratic flow harmonics of pions, kaons, and protons present similar mass ordering as the case for the elliptic flow [156]. In Ref. [109], the PKU group implemented the iEBE-VISHNU hybrid model with the AMPT initial conditions to investigate the flow harmonics of identified hadrons $v_n(pT)$ ($n = 2, 3, 4$) at the LHC. After tuning the Gaussian

smearing factor for initial energy decompositions and the QGP shear viscosity, the differential v_n of all charged hadrons can be nicely described by the iEBE-VISHNU simulations. As shown in Fig. 3, iEBE-VISHNU also nicely describes the v_n data of pions, kaons, and protons, especially when reproducing correct mass orderings for these different flow harmonics. Reference [109] also showed the pure hydrodynamic simulations do not generate enough mass splittings between the v_n of pions and protons. The late hadronic evolution in the iEBE-VISHNU re-distributes the anisotropy flow to various hadron species through the microscopic hadronic scatterings which enhances the v_n mass splitting between pions and protons and leads to a nice description of the experimental data [109].

4.1.1 The issues of bulk viscosity

For simplicity, the early semi-quantitative extraction of the QGP shear viscosity at the RHIC and the LHC neglects the effects from bulk viscosity.⁴ The (0+1)-d viscous hydrodynamic calculations without transverse expansion [157, 158] suggested that, for a uniform system undergoing rapid boost-invariant longitudinal expansion, the bulk pressures can turn into pretty large values, leading to mechanically unstable fluid with negative effective pressure. The 2+1-d viscous hydrodynamics with single shoot simulations showed that the bulk viscosity also suppresses the elliptic flow as the shear viscosity [159–163] but with smaller efforts due to the critical slowing down near the QCD phase transition [159]. Recently, the 3+1-d event-by-event simulations from MUSIC found that the bulk viscosity largely influenced the average transverse momentum

⁴ At the LHC and top RHIC energies, the heat conductivity can be neglected due to the almost vanishing net baryon density.

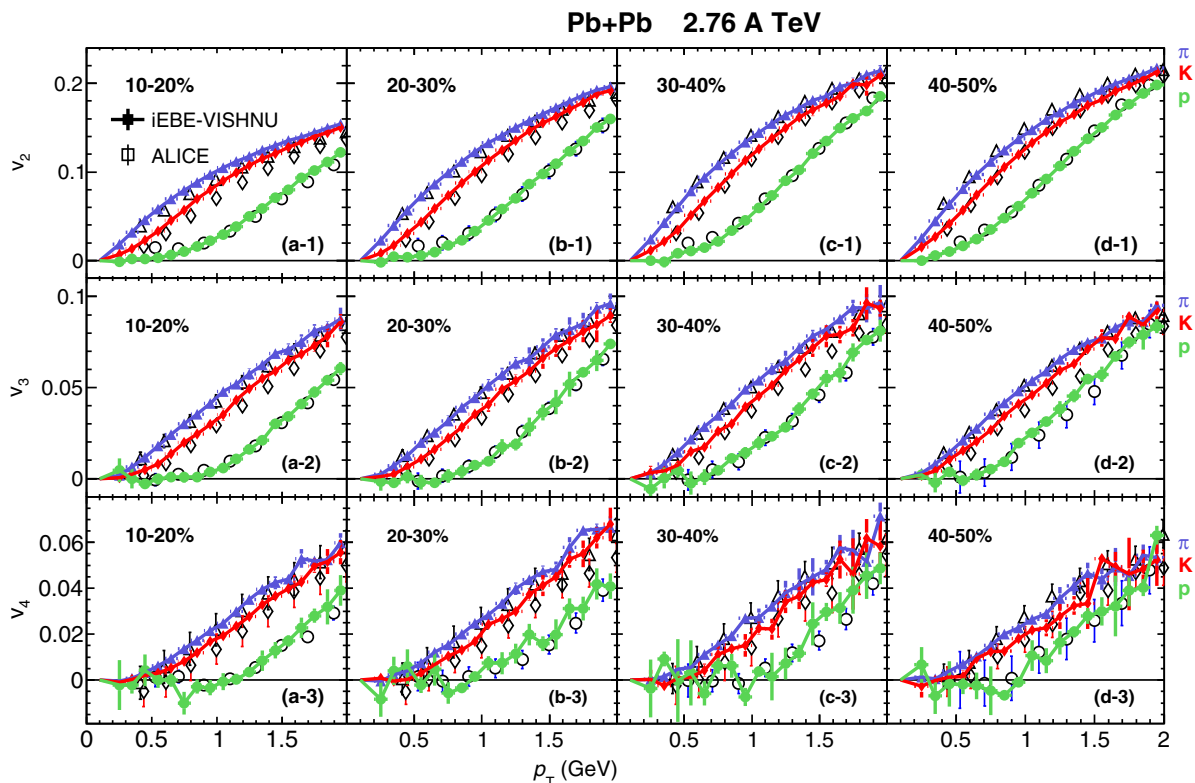


Fig. 3 (Color online) $v_n(pT)$ ($n = 2, 3, 4$) of pions, kaons, and protons in 2.76 A TeV Pb–Pb collisions, calculated from iEBE-VISHNU with AMPT initial conditions [109]. The experimental data are taken from the ALICE paper [150, 151]

of identified hadrons [164]. For the MUSIC calculation with the IP-Glasma initial condition, the fitting of the pT spectra is largely improved by a properly chosen bulk viscosity, which also leads to a consistent description of other soft hadron data, such as the integrated and differential flow harmonics at various centralities in 2.76 A TeV Pb–Pb collisions.

4.2 Quantitative extractions of the QGP shear and bulk viscosity with massive data evaluations

For the flow calculations and predictions at RHIC or at the LHC, most of the hydrodynamics/hybrid model simulations, with different types of initial conditions, input a constant value of the specific QGP shear viscosity and neglect the effects of bulk viscosity. The early model calculations also revealed that the averaged QGP shear viscosity changes with the collision energies, which is slightly larger at the LHC than at RHIC [19, 123, 131, 154]. It is thus very important to extract a temperature-dependent QGP shear viscosity, $(\eta/s)_{QGP}(T)$, from the massive soft hadron data in relativistic heavy ion collisions. For the purposes of massive data evaluations, the Livermore group developed the CHIMERA algorithm (a comprehensive heavy ion model evaluation and reporting algorithm) and

extracted the initial temperature and the QGP shear viscosity from a simultaneous fit of the pT spectra, elliptic flow, and HBT radii in 200 A GeV Au + Au collisions [165]. Note that these early massive hydrodynamic simulations around 2012 assume the QGP shear viscosity is a constant value and the bulk viscosity is zero together with an input of the traditional MC-Glauber initial condition, which has been ruled out by some later flow measurements.

To avoid the limitations of simultaneously tuning multiple free parameters in the early work [165], the Duke-OSU group implemented the Bayesian method to the event-by-event hybrid model simulations [166] and then quantitatively estimated the properties of the QGP through a multi-parameter model to data comparison, using the parametric T_RENTo initial conditions [167]. Using the newly developed massive data evaluating techniques, the global fitting of the multiplicity, transverse momentum, and flow data at the LHC constrain the free parameters in the T_RENTo model, which also give an extracted temperature-dependent specific shear viscosity and bulk viscosity.

Figure 4 shows the estimated temperature-dependent shear viscosity, $(\eta/s)(T)$, from the DUKE-OSU group, obtained from the massive data fitting in 2.76 A TeV Pb+Pb collisions. The blue line is the median with a blue band showing the 90% credible region. Correspondingly, a

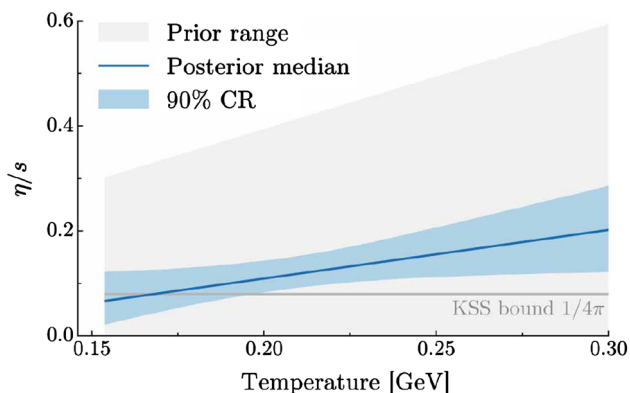


Fig. 4 (Color online) Estimated temperature dependence of the shear viscosity (η/s)(T) above the QCD phase transition (for $T_c > 154$ MeV), obtained from a multi-parameter model to data comparison [167]

nonzero bulk viscosity with a peak near the QCD phase transition has also been extracted simultaneously (For details, please refer to [167]). With these extracted QGP transport coefficients and other extracted most probable parameters, the event-by-event hybrid simulations give an excellent overall fit for the multiplicities and mean pT of all charged and identified hadrons and the integrated v_n ($n = 2, 3, 4$) of all charged hadrons from the most central collisions to the peripheral collisions in Pb–Pb collisions at the LHC, as shown in Fig. 5.

Note that this extracted $\eta/s(T)$, within the uncertainty band, is compatible with the well-known KSS bound, $\eta/s < 1/4\pi$ [168–170], which also supports several early semi-quantitative extractions of the QGP viscosity at RHIC and the LHC. For example, the extracted specific QGP

viscosity, $\frac{1}{4\pi} < (\eta/s)_{QGP} < 2.5 \times \frac{1}{4\pi}$, from the VISHNU calculations with MC-Glauber and MC-KLN initial conditions [148, 153] and the implemented $\eta/s = 0.095$ (with the same bulk viscosity parametrization) in the MUSIC simulations with the IP-Glasma initialization [164] are both consistent with this quantitative extracted results from the DUKE-OSU collaborations. The early EKRT viscous hydrodynamic calculations for the flow data at RHIC and the LHC also prefer a temperature-dependent $\eta/s(T)$ with a positive slope [112].

Compared with the early extraction of the QGP viscosity with specific initial condition, Ref. [167] implemented the parametric $T_{R}ENTo$ model that could smoothly interpolate among various initial condition schemes through tuning the related parameters. It is thus an ideal initial-state model for the massive model-to-data comparison, which helps to make a simultaneous constraint for the initial conditions and the QGP transport coefficients. It was found that the initial entropy deposition from the constrained $T_{R}ENTo$ model with fixed parameters is approximately proportional to the geometric mean of the participant nuclear densities, which gives similar scaling to the successful EKRT and IP-Glasma initial conditions.

In Ref. [172], the Bayesian statistical analysis was extended to the massive data fitting in Au–Au collisions at $\sqrt{s_{NN}} = 19.6, 39$ and 62.4 GeV. It was found that the extracted constant QGP specific shear viscosity, η/s , decreases with the increase of collision energy, which shows a similar result obtained from the early hybrid model calculations [123]. In the future, a combined massive data fitting at RHIC (including BES) and the LHC will give more precise temperature-dependent transport coefficients of the QGP.

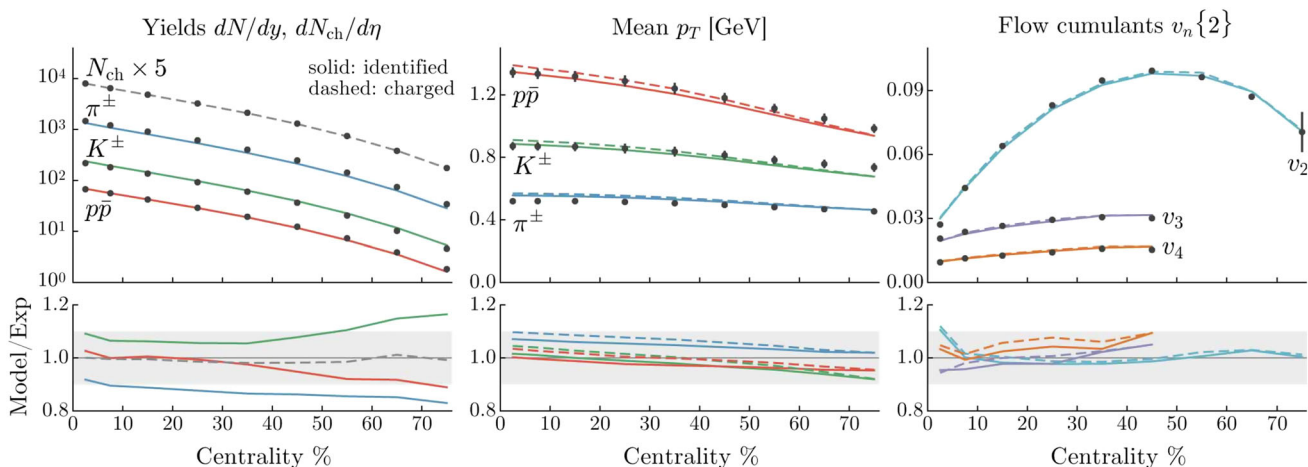


Fig. 5 (Color online) Multiplicities, mean pT of all charged and identified hadrons and the integrated v_n ($n = 2, 3, 4$) of all charged hadrons in 2.76 A TeV Pb–Pb collisions, calculated from event-by-

event hybrid model with the high-probability parameters extracted from the massive data fitting [167]. The data are from the ALICE experiment [24, 171]

5 Initial-state fluctuations and final-state correlations

The event-by-event initial-state fluctuations of the created QGP fireballs lead to the final-state correlations, which produce the elliptic flow, triangular flow, and other higher-order flow harmonics as observed in the experiments at RHIC and the LHC [23–26, 173–176]. The QGP viscosity largely suppresses flow harmonics at different order v_n . As reviewed in the last section, the transport properties of the QGP fireball have been extracted from this flow data with the event-by-event hydrodynamics / hybrid model simulations [30, 110, 154]. In this section, we will review other flow observables, such as event-by-event v_n distribution, the event-plane correlations, the correlations of flow harmonics, that are more sensitive to the details of model calculations, which may provide additional constrains for the initial-state models and for the extracted QGP transport coefficients in the future.

5.1 Event-by-event v_n distribution

The flow harmonics, v_n , are generally measured within a base of the event average, which mainly reflects the hydrodynamic response to the averaged initial eccentricity coefficients, ε_n , within some centrality bin. With a large amount of particles produced per event at the LHC, a direct measurement of the event-by-event v_n distribution becomes possible, which provides more information on the initial-state fluctuation and the underlying probability density function. Around 2012, the ATLAS Collaboration made the first measurement of the event-by-event distributions of v_n ($n = 2, 3, 4$) in Pb–Pb collisions at $\sqrt{s_{NN}} = 2.76$ TeV [29]. Figure 6 shows the MUSIC hydrodynamic calculations nicely describe the ATLAS data with the IP-Glasma initial conditions. It also shows, for $n = 2$ and 3, the rescaled $v_n/\langle v_n \rangle$ distributions mostly follow the $\varepsilon_n/\langle \varepsilon_n \rangle$ distributions from the initial state, which are not sensitive to the details of the hydrodynamic evolution [30]. Due to the mode couplings effects for higher flow harmonics, the distributions of $v_4/\langle v_4 \rangle$ are not necessarily follow $\varepsilon_4/\langle \varepsilon_4 \rangle$. The hydrodynamic evolution balances the distributions of $v_4/\langle v_4 \rangle$ making a nice description of the experimental data. In Ref. [29], the measured v_n distributions were compared with the ε_n distributions from MC-Glauber and MC-KLN models, which demonstrated certain deviations between model and data for most of the centrality classes. The v_n distributions thus provide strong constrains on the initial-state models, which do not favor the MC-Glauber and MC-KLN initial conditions.

The ATLAS measurements can also be used to examine the underlying *p.d.f.* of the v_n distributions. The most

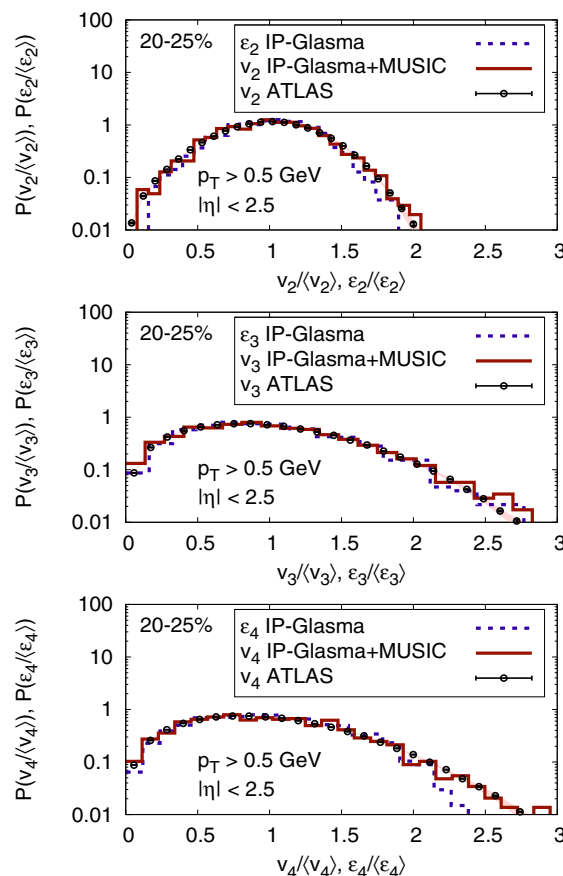


Fig. 6 (Color online) Scaled event-by-event distributions of v_n ($n = 2, 3, 4$) from the MUSIC simulations with the IP-Glasma initial conditions [30], together with a comparison with the ATLAS data [29]

popular parameterizations are the Bessel-Gaussian distributions [178]:

$$p(v_n) = \frac{v_n}{\sigma^2} I_0\left(\frac{v_n v_0}{\sigma^2}\right) \exp\left(-\frac{v_0^2 + v_n^2}{2\sigma^2}\right), \tag{25}$$

where v_0 is the anisotropic flow from the reaction plane, Ψ_{RP} , and σ is the anisotropic flow fluctuation. It was reported that the Bessel–Gaussian distribution could nicely describe the v_2 distributions for mid-central collisions [178, 179]. Without the constraint of $\varepsilon_2 < 1$ for each event, it is not expected to work well in peripheral collisions [180]. To fix this problem, a new function, named “Elliptic Power” distribution, was proposed in Ref. [180], which is expressed as:

$$p(v_n) = \frac{\alpha v_n}{\pi} (1 - v_0^2)^{\alpha + \frac{1}{2}} \int_0^{2\pi} \frac{(1 - v_n^2)^{\alpha - 1} d\phi}{(1 - v_0 v_n \cos \phi)^{2\alpha + 1}}, \tag{26}$$

where α quantifies the fluctuations and v_0 has the same meaning as the Bessel-Gaussian parameterizations. As a promising candidate of underlying *p.d.f.* of v_n distribution, the Elliptic-Power function can nicely describe the event-

by-event v_2 and v_3 distributions [180, 181]. However, it cannot give an equally nice fitting for these distributions of higher flow harmonics ($n \geq 4$), which are largely influenced by the nonlinear hydrodynamic response. For details, please refer to [180, 181].

5.2 De-correlations of the flow vector V_n

Recently, it was realized that the produced particles at different transverse momenta, p_T , and rapidity y do not share a common flow angle or event plane. Such transverse momentum and rapidity dependent flow angles fluctuate event-by-event, which also breaks the factorizations of the flow harmonics [38, 39]. To evaluate the de-correlations of the flow vector, especially on the transverse momentum dependence, two new observables, $v_n\{2\}/v_n[2]$, and the factorization ratio, r_n , have been proposed, which are defined as:

$$\frac{v_n\{2\}}{v_n[2]}(p_T^a) = \frac{\langle v_n^a v_n \cos[n(\Psi_n^a - \Psi_n)] \rangle}{\langle v_n^a v_n^a \rangle^{1/2} \langle v_n v_n \rangle^{1/2}}; \quad (27)$$

$$r_n = \frac{\langle v_n^a v_n^b \cos[n(\Psi_n^a - \Psi_n^b)] \rangle}{\langle v_n^a v_n^a \rangle^{1/2} \langle v_n^b v_n^b \rangle^{1/2}} \quad (28)$$

where v_n^a , Ψ_n^a (or v_n^b , Ψ_n^b) are the n th-order flow harmonics and the flow angle at the transverse momentum p_T^a (or p_T^b). The p_T dependent fluctuations of the flow angle and magnitude make $v_n\{2\}/v_n[2] < 1$ and r_n deviated from 1. As shown in Fig. 7, these deviations from unity have already been observed in experiment and qualitatively described by the related hydrodynamic calculations [38], which indicates the existence of the p_T dependent fluctuations of flow angle and magnitude.

The fluctuations in the longitudinal direction have also been investigated both in experiment and in theory [40, 183–186]. Reference [184] found that the final-state de-correlations of the anisotropic flows in different pseudo-

rapidity regime is associated with the spatial longitudinal de-correlations from the initial state. It also predicted a larger longitudinal de-correlation at RHIC than the ones at the LHC, which provide opportunities to further study the longitudinal fluctuation structures of the initial stage.

5.3 Event-plane correlations

The correlations between different flow vectors could reveal more information on the initial-state fluctuations and the hydrodynamic response [187]. In Ref. [31], the ATLAS Collaboration has measured the event-plane correlations among two or three event-plane angles, $\langle \cos(c_n n \Psi_n + c_m m \Psi_m) \rangle$ and $\langle \cos(c_n n \Psi_n + c_m m \Psi_m + c_h h \Psi_h) \rangle$, in 2.76 A TeV Pb–Pb collisions and observed several different centrality-dependent trends for these correlators. It was also reported that the MC-Glauber model, which only involves the correlations from the initial state, cannot reproduce the trends for many of these correlators [31]. Using event-by-event hydrodynamics with MC-Glauber and MC-KLN initial conditions, Qiu and Heinz have systematically calculated the event-plane correlations and demonstrated that the hydrodynamic evolution is essential for an overall qualitative description of various flow angle correlations [32]. Figure 8 presents the model to data comparisons for several selected correlation functions which shows that although correlation strength is sensitive to the initial conditions and the QGP shear viscosity, hydrodynamics successfully reproduces the centrality-dependent trend of these event-plane correlations. In contrast, the correlations of the initial eccentricity plane show large discrepancies with the measured and calculated event correlations of the final produced particles, including magnitudes, qualitative centrality dependence, and even in signs [32]. In Ref. [31, 188], it was found that the AMPT simulations are also able to roughly reproduce the ATLAS data with well-tuned parameters. These different model

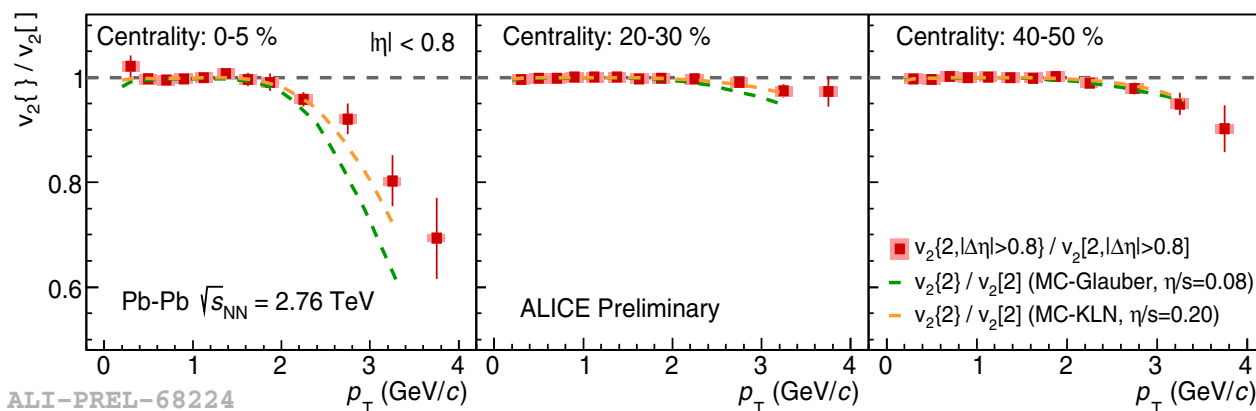


Fig. 7 (Color online) The ratio $v_n\{2\}/v_n[2]$ at various centralities in 2.76 A TeV Pb–Pb collisions. The theoretical lines are calculated from VISH2+1 with MC-Glauber and MC-KLN initial conditions [38], and the experimental data are measured by the ALICE collaborations [177]

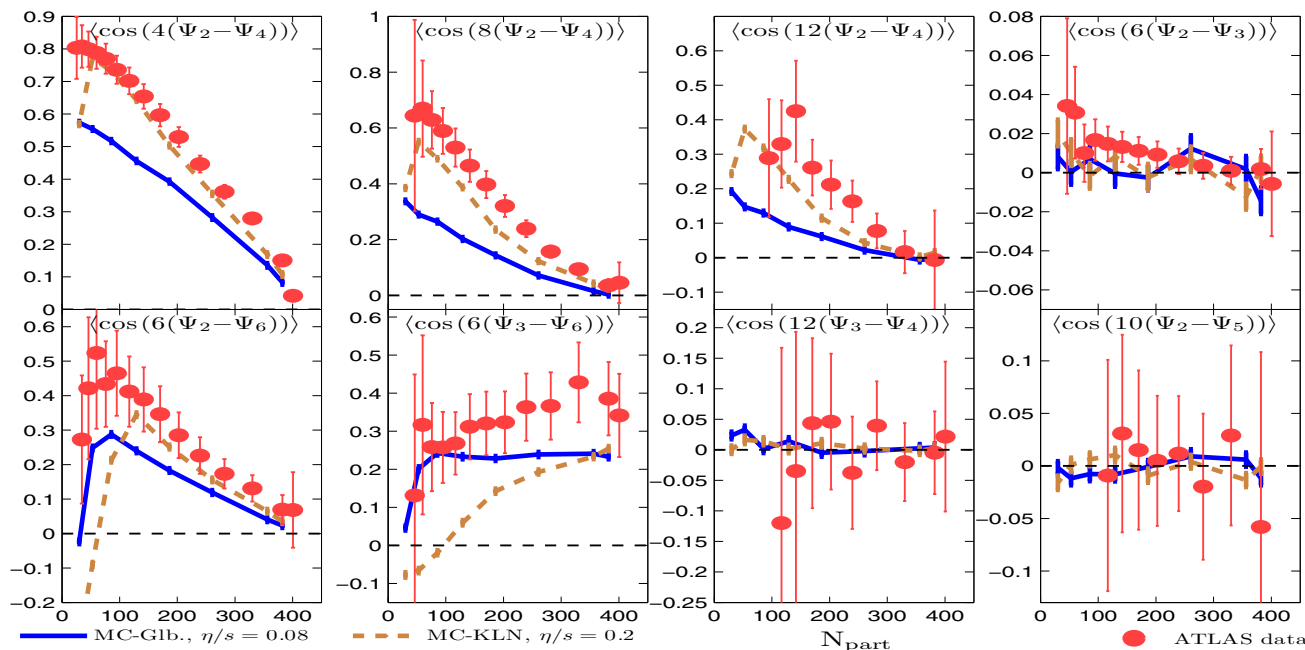


Fig. 8 (Color online) Centrality-dependent event-plane correlations calculated from event-by-event VISH2 + 1 hydrodynamic simulations with MC-Glauber and MC-KLN initial conditions [32]. The data are measured by the ATLAS collaborations [31]

calculations, involving final-state interactions [31, 32, 188], demonstrate that the observed event-plane correlations are not solely driven by the initial geometry, but are largely influenced by the complicated evolution of the QGP fireball.

Using a nonlinear response formalism, Ref. [182] calculated the event-plane correlations from the initial energy density but expanded with the cumulants method, which roughly reproduces the centrality-dependent trends of several selected correlations. It is also found that the nonlinear response of the medium has a strong influence on

these related correlators. As shown in Fig. 9, the linear response alone is not able to describe the $\langle \cos(4(\Psi_2 - \Psi_4)) \rangle$ and $\langle \cos(2\Psi_2 + 3\Psi_3 - 5\Psi_5) \rangle$ correlators, while a good description of the data can be achieved after combining the contributions of both linear and nonlinear response.

5.4 Correlations of flow harmonics

Besides the event-plane correlations, the correlations between different flow harmonics are other important

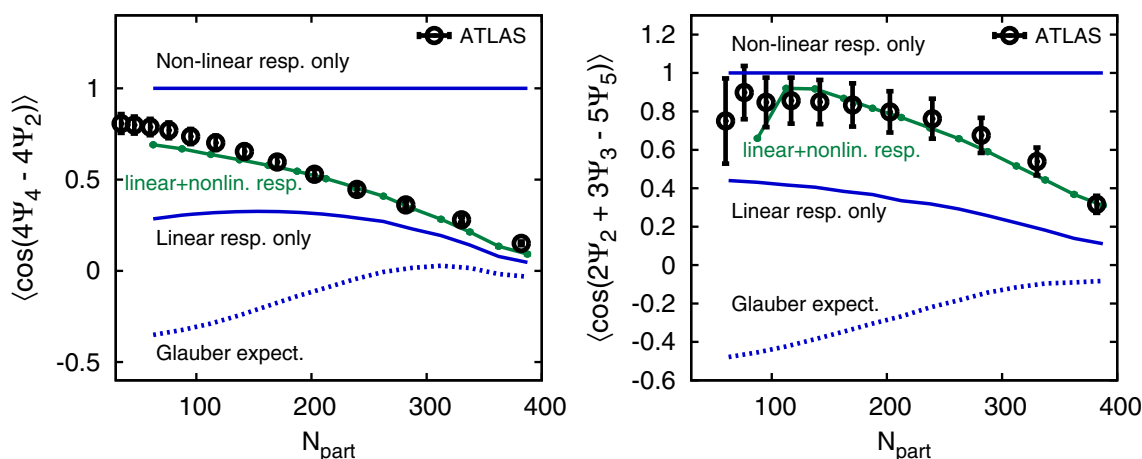


Fig. 9 (Color online) The separate contributions from linear, nonlinear, and combined response to the event-plane correlations [182] together with a comparison with the ATLAS data [31]

observables closely related to the corrections of the flow vectors that could further reveal the initial-state correlations and the hydrodynamic response. Using the Event-Shape Engineering (ESE) [189], the ATLAS Collaboration firstly measured the correlations between flow harmonics based on the 2-particle correlations and found that v_2 and v_3 are anti-correlated and v_2 and v_4 are correlated [33].⁵ Recently, a new observable, called Symmetric Cumulants $SC^v(m, n)$, was proposed as an alternative approach to measure the correlations between different flow harmonics. It is defined as $SC^v(m, n) = \langle v_m^2 v_n^2 \rangle - \langle v_m^2 \rangle \langle v_n^2 \rangle$ and can be measured by the multi-particle cumulant method. The related Monte Carlo model simulations imply that $SC^v(m, n)$ is insensitive to the non-flow effects [34]. Besides, $SC^v(m, n)$ is independent on the symmetry plane correlations by design [146].

Figure 10 (left) shows the centrality-dependent symmetric cumulants $SC^v(4, 2)$ and $SC^v(3, 2)$ in 2.76 A TeV Pb–Pb collisions, measured from ALICE [34] and calculated from the EKRT event-by-event hydrodynamics [112]. The positive values of $SC^v(4, 2)$ and negative values of $SC^v(3, 2)$ are consistent with the early observation from ATLAS [33], which also illustrates that v_2 is anti-correlated with v_3 , but is correlated with v_4 . A comparison between the model calculations and the experimental data in Fig. 10 also shows that, although hydrodynamics could successfully reproduce the integrated flow harmonics, v_n , it can only qualitatively, but not quantitatively, describe the correlations between these harmonics.

In Ref. [36], the symmetric cumulants $SC^v(m, n)$ and other related observables have been systematically calculated by the event-by-event viscous hydrodynamics VISH2+1 with a focus on investigating the influences from different initial conditions and QGP shear viscosity. Like the case of the early EKRT hydrodynamic simulations, all of these VISH2+1 simulations with MC-Glauber, MC-KLN, and AMPT initial conditions could capture the sign and centrality dependence of $SC^v(4, 2)$ and $SC^v(3, 2)$, but not be able to archive a simultaneous quantitative description of these two symmetric cumulants for all centrality intervals. Compared with the individual flow harmonics v_2 and v_3 , the symmetric cumulants $SC^v(4, 2)$ and $SC^v(3, 2)$ are more sensitive to the details of the theoretical calculations. Reference [36] also predicted other symmetric cumulants $SC^v(5, 2)$, $SC^v(5, 3)$, and $SC^v(4, 3)$ and found that v_2 and v_5 are correlated, v_3 and v_5 are correlated, v_3 and v_4 are anti-correlated for various centralities.

In order to get rid of the influences from individual flow harmonics, it was suggested to normalize $SC^v(m, n)$ by dividing the products $\langle v_m^2 \rangle \langle v_n^2 \rangle$ [34]. Figures 10 (right) and 11a, b, c, g, h plot the normalized symmetric cumulants $NSC^v(n, m)$ ($NSC^v(n, m) = SC^v(n, m) / (\langle v_n^2 \rangle \langle v_m^2 \rangle)$) in 2.76 A TeV Pb–Pb collisions. $NSC^v(4, 2)$ exhibits a clear sensitivity to the initial conditions and the $\eta/s(T)$ parameterizations, which could provide additional constrains for the initial geometry and the transport coefficients of the hot QCD matter. In contrast, $NSC^v(3, 2)$ is insensitive to the detailed setting of η/s and the used initial conditions. Figure 11 also shows that the values of $NSC^v(3, 2)$ is compatible to the ones of $NSC^e(3, 2)$ from the initial state due to the linear response of v_2 (v_3) to ε_2 (ε_3). Note that these different $NSC^v(3, 2)$ curves in Fig. 11g are almost overlap with each other, which also roughly fit the normalized ALICE data. In contrast, the predicted $NSC^v(4, 2)$, $NSC^v(5, 2)$, and $NSC^v(5, 3)$ are sensitive to both initial conditions and η/s . Due to the nonlinear hydrodynamic response, $NSC^v(4, 3)$ does not necessarily follow the sign of $NSC^e(4, 3)$ for some certain initial conditions.

In a recent work [35], the $NSC^v(m, n)$ are expressed in terms of the symmetry plane correlations and moments of v_2 and v_3 . Considering the relative flow fluctuations of v_3 are stronger than v_2 , one expects smaller values for $NSC^v(5, 2)$ compared to $NSC^v(5, 3)$, as shown in Fig. 11. On the other hand, it was predicted that $NSC^v(m, n)$ involving v_4 and v_5 increases with η/s in the same way as the symmetry plane correlations [190, 191], which qualitatively agrees with the results in Fig. 11 from most central collisions to semi-peripheral collisions.

As discussed above, the low flow harmonics, v_2 or v_3 , is mainly determined by a linear response to the initial eccentricity ε_2 or ε_3 , while higher flow harmonics (v_n with $n > 3$) not only contains the contributions from the linear response of the corresponding ε_n , but also has additional contributions from lower order initial anisotropy coefficients. These additional contributions are usually called nonlinear response of higher flow harmonics [192, 193]. In Ref. [35], it was proposed that a direct connection between the symmetry plane correlations and the flow harmonic correlations $NSC^v(m, n)$ could be built from the nonlinear hydrodynamic response of higher flow harmonics. Besides, the past hydrodynamic calculations have shown that the contributions of nonlinear response can explain the symmetry plane correlations and its centrality dependence [37, 193]. Recently, the proposed nonlinear hydrodynamic coefficient, χ_{mn} [193], has been systematically studied and measured [37, 194, 195], which could be used to further constrain the initial conditions and η/s and to provide a better understand of the correlations between different flow harmonics.

⁵ For the related qualitative investigations from hydrodynamics, please refer to [37].

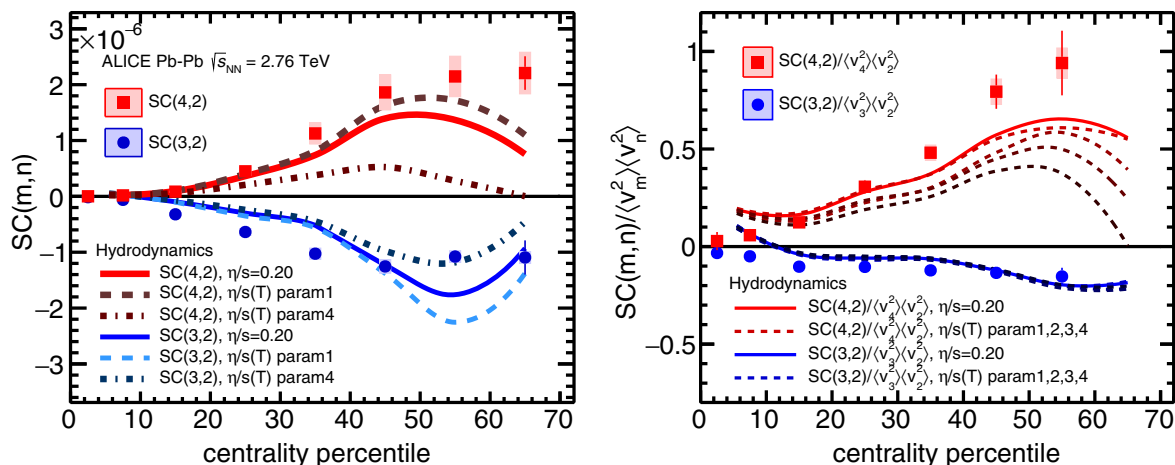


Fig. 10 (Color online) The centrality dependence of symmetric cumulants SC(4, 2) and SC(3, 2) in 2.76 A TeV Pb–Pb collisions [34]

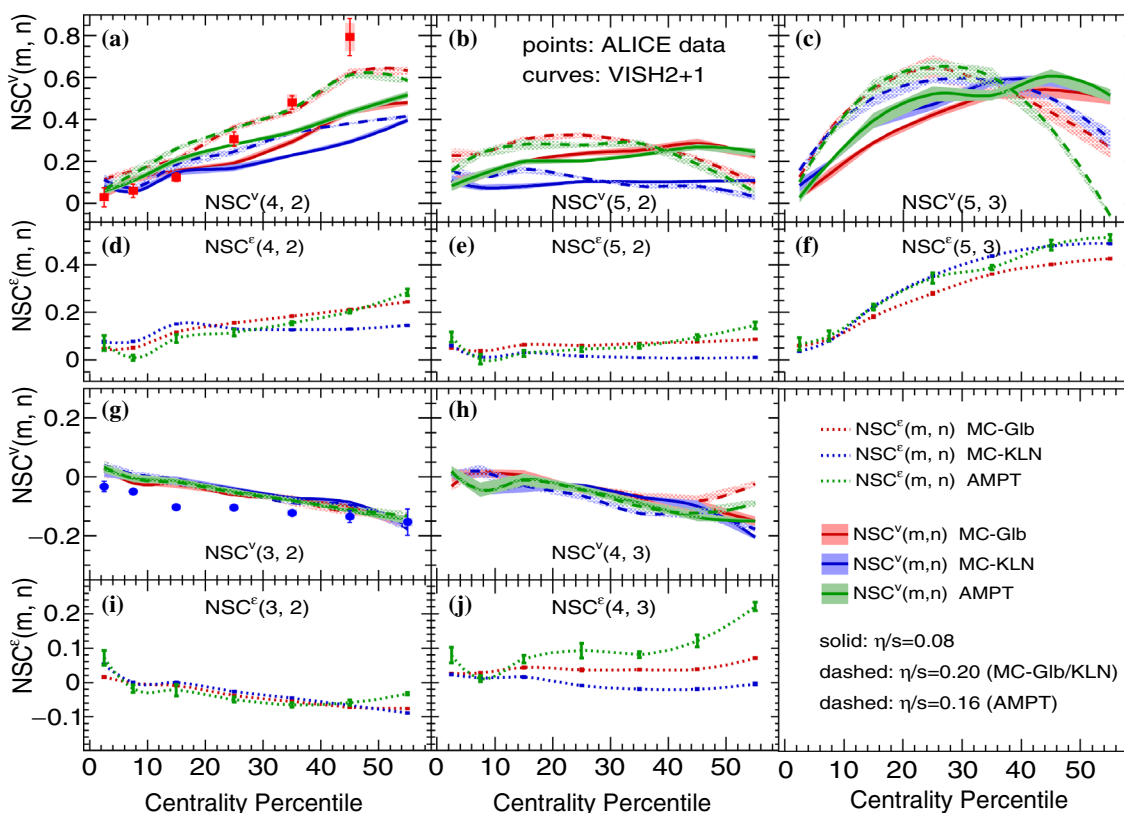


Fig. 11 (Color online) The centrality dependence of normalized symmetric cumulants $NSC^v(m, n)$, and the corresponding normalized symmetric cumulants of the initial eccentricity coefficients

$NSC^e(m, n)$ in 2.76 A TeV Pb–Pb collisions, calculated from event-by-event VISH2+1 simulations with MC-Glauber, MC-KLN, and AMPT initial conditions [36]

6 Correlations and collective flow in small systems

6.1 p–Pb collisions at $\sqrt{s_{NN}} = 5.02$ TeV

High-energy proton-lead (p–Pb) collisions at the LHC were originally aimed to study the cold nuclear matter

effects and provide the corresponding reference data for Pb–Pb collisions. However, lots of unexpected collective phenomena have been observed in the experiments. For example, the measured two-particle correlations showed a symmetric double ridge structure on both the near- and away-side in high-multiplicity p–Pb collisions at $\sqrt{s_{NN}} = 5.02$ TeV [41–44]. Besides, negative 4- and 8-particle

cumulants and positive 6-particle cumulants have been observed in the high-multiplicity events [43–45]. In particular, all the multi-particle cumulants (including 4-, 6-, and 8-particles cumulants) are compatible to the ones obtained from the all-particle correlations with Lee–Yang Zero’s method, which corresponds to $v_2\{4\} \approx v_2\{6\} \approx v_2\{8\} \approx v_2\{\text{LYZ}\}$ [44], as shown in Fig. 12 (This observation has also been confirmed by the later ATLAS [43] and ALICE Collaborations [45] measurements). Meanwhile, the obtained v_2 from two or four-particle cumulants are comparable to the ones from Pb–Pb collisions at 2.76 TeV [43, 44, 46, 196]. Recently, the ALICE collaboration has extended the investigation of anisotropic collectivity via azimuthal correlations of identified hadrons [46, 47]. A typical mass-ordering feature among the v_2 of pions, kaons and protons is observed in high-multiplicity p–Pb collisions [46]. Similarly, the CMS Collaboration found a v_2 mass ordering between K_S^0 and $\Lambda(\bar{\Lambda})$ [47].

There are many theoretical efforts attempting to provide explanation for the flow-like behavior of the p–Pb collisions. In general, they can be divided into two big categories that don’t involve the final-state evolution of the medium but only account for initial-state effects [197–205], and that includes the final-state interactions, such as the hydrodynamics or kinetic model description [48–54, 206–211]. In this section, we will focus on reviewing the hydrodynamic calculations as well as the kinetic model investigations on the flow-like signals in the small p–Pb systems.

6.1.1 Results from hydrodynamic simulations

Hydrodynamics is a useful tool to simulate the collective expansion of the created systems and quantitatively study and predict the final flow observable. Recently, the holographic duality calculations have shown that the size of the produced droplet is $\sim 1/T_{\text{eff}}$ [212, 213], which indicates that hydrodynamics is possibly applicable for the small systems created in the high-energy p–Pb and p–p collisions. Using 3+1-d hydrodynamic or hybrid model simulations, different groups have systematically studied the multiplicities, mean pT , final-state correlations, and related flow data in p–Pb collisions at $\sqrt{s_{\text{NN}}} = 5.02$ TeV [48–54]. In general, these hydrodynamic calculations could semi-quantitatively describe these different soft hadron data, which support the observation of collective flow in experiments of high-energy p–Pb collisions.

Figure 13 (left) presents the hydrodynamic calculations for flow coefficients v_2 and v_3 of all charged hadrons in high-multiplicity p–Pb collisions, which gives a rough fit of the data from the CMS collaborations [50]. It was also

found that such fluid evolution also developed in the radial flow, which leads to a flatter transverse momentum spectra for various hadron species. As shown in Ref. [50], the average transverse momentum of the identified hadrons in p–Pb collisions can be consistently fitted by the hydrodynamic simulations. In contrast, the HIJING model, without any collective expansion, fails to describe the data. In the hydrodynamic language, the interaction between radial and elliptic flow re-distribute, the total momentum anisotropy to various hadron species, leading to a mass ordering of the flow harmonics. Figure 13 (right) shows that the hydrodynamic simulations roughly reproduce the v_2 mass ordering of pions, kaons, and protons. Note that, other hydrodynamic calculations with different initial conditions and transport coefficients also obtained similar results. For details, please refer to Refs. [51–54].

Reference [214] has shown that, in order to reproduce the multiplicity distribution of p–Pb collisions using the hydrodynamic calculations with Glauber initial conditions, the implementation of additional negative binomial fluctuations is necessary. Correspondingly, initial eccentricities are also modified which leads to a simultaneous fit of the $v_2\{2\}$ and $v_2\{4\}$ data. In contrast, the early IP-glasma initial condition generates the initial energy distributions with an imprinted spherical shape of protons, which yields a very small v_2 for the p–Pb collision systems [54]. This motivates the recent investigations of the proton structure within the saturation framework, which indicates that the shape of the protons also fluctuates event-by-event [215, 216].

Note that the flow-like signals have also been observed in d–Au and ^3He –Au collisions at RHIC. Compared to the p–A collisions at the LHC, the d–Au and ^3He –Au collisions provide controlled initial geometry deformations, which are less sensitive to the details of initial-state models and are helpful to check the hydrodynamic calculations. Recently, the STAR and PHENIX collaboration has measured the elliptic flow v_2 in d–Au collisions at $\sqrt{s_{\text{NN}}} = 200$ GeV and the elliptic and triangular flow v_2 and v_3 in ^3He –Au collisions at $\sqrt{s_{\text{NN}}} = 200$ GeV [217–220]. The hydrodynamic calculations from different groups, using various initial conditions and the QGP shear viscosity, roughly described these extracted flow data. It was also found that v_2 and v_3 follows ε_2 and ε_3 from the initial state, which gives a support for the collective expansion in these small systems created at RHIC [51, 52, 221–223].

Compared with the Pb–Pb collisions, the initial sizes of the created systems in p–Pb collisions are much smaller. The subsequent collective expansion is expected to enlarge the size of the fireball, where the corresponding radii at the freeze-out can be measured by the Hanbury–Brown–Twiss (HBT) correlations. In Ref. [224], the ALICE collaboration

Fig. 12 (Color online) Multiplicity dependence of v_2 , obtained from the Fourier decomposition of 2-particle azimuthal correlations, from multi-particle cumulants, and via the LYZ method, in Pb–Pb collisions at $\sqrt{s_{NN}} = 2.76$ TeV (left) and p–Pb collisions at $\sqrt{s_{NN}} = 5.02$ TeV (right) [44]

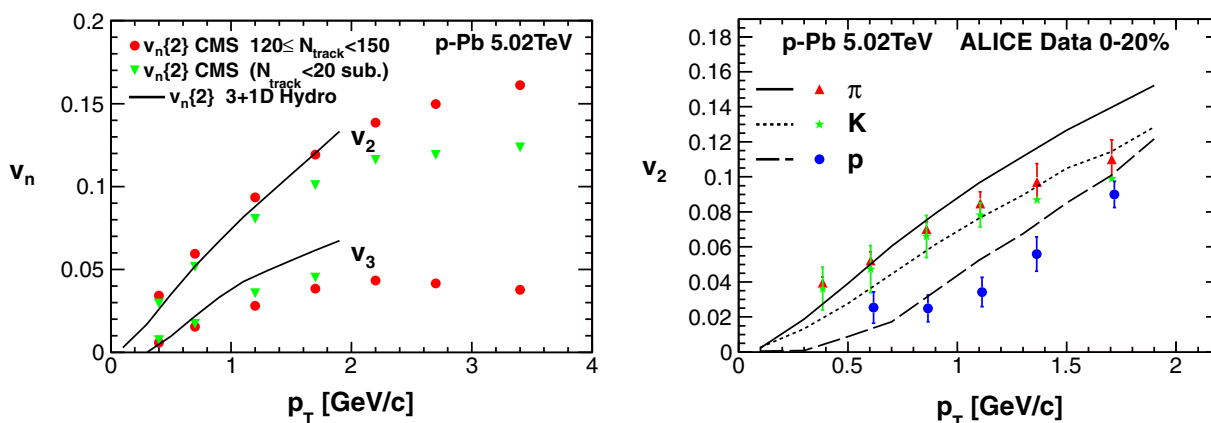
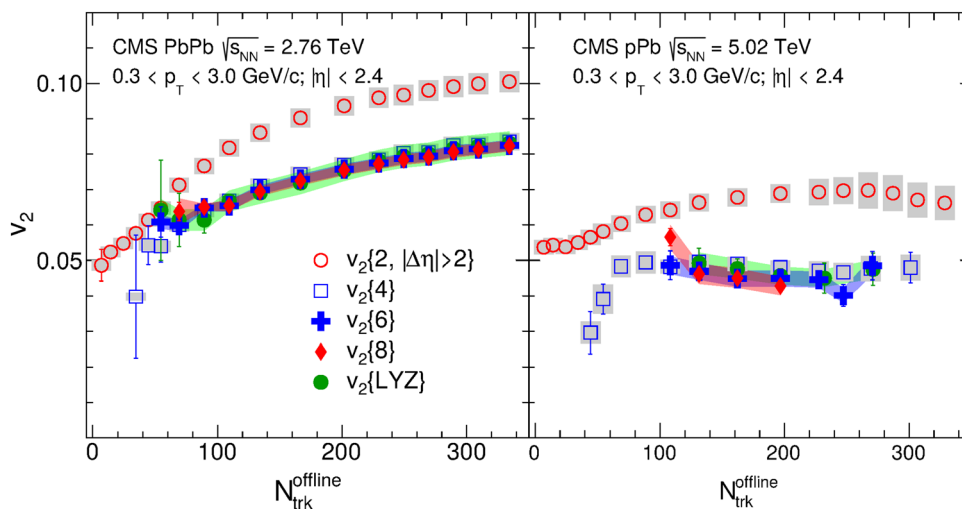


Fig. 13 (Color online) The hydrodynamic calculations of the elliptic and triangular flow coefficient of all charged particles (left panel) and elliptic flow of identified hadrons (right panel) in p–Pb collisions at

$\sqrt{s_{NN}} = 5.02$ TeV [50], together with a comparison with the CMS [196] and ALICE data [46]

has measured the three-dimensional pion femtoscopic radii in p–Pb collisions at $\sqrt{s_{NN}} = 5.02$ TeV, which showed that the size of the p–Pb systems is in between the ones obtained from the p–p collisions and peripheral Pb–Pb collisions. In general, the hydrodynamic calculations could roughly describe the HBT measurements, while the quantitative values from different model calculations are sensitive to the initial conditions and the imprinted initial sizes of the created fireball [223, 225, 226].

In Ref. [227], the validity of hydrodynamics for large Pb–Pb and small p–Pb systems at the LHC has been evaluated through tracing the space-time evolution of the Knudsen number. It was found for Pb–Pb collisions, hydrodynamic simulations with $\eta/s \sim 1/4\pi$ are always within the validity regime with the Knudsen numbers well below one. However, the related simulations for smaller p–A systems shows that the hydrodynamic descriptions have broken down at the $T_{dec} = 100$ MeV freeze-out boundary, even when using a minimum QGP shear viscosity as a

input. Although such investigations will not preclude the collective flow and final-state interactions, it is worthwhile to explore the physics of the small p–Pb systems within other frameworks beyond hydrodynamics.

6.1.2 Results from other approaches

Without the final-state interactions, the long-range rapidity correlations in high-energy p–p and p–Pb collisions have been calculated with the framework of Color Glass Condensate (CGC), which shows a good agreement with the di-hadron data from the CMS, ATLAS, and ALICE [197–200]. However the odd harmonics data disfavor these early CGC calculations without the rescattering contributions [201]. Without a proper hadronization procedure, such calculations can also not predict the flow data of the identified hadrons. Recently, it was proposed that the presence of the colored domains inside the proton and the nucleus breaks rotational invariance, which helps to

generate elliptic and triangular flow during the scatterings between a dilute projectile of valence quarks and the nucleus [202–205]. An alternative approach is the classical Yang-Mills simulations, which treat both the proton and nucleus as dense QCD objects with high gluon occupancy and are more appropriate to describe the early time evolution of the created p–Pb systems in the high-multiplicity events. Within such framework, Schenke and his collaborators have calculated the single and double inclusive gluon distributions and extracted the associated pT dependent elliptic and triangular flow of gluons in high-energy p–A collisions [228]. They found that the final-state effects in the classical Yang-Mills evolution build up a nonzero triangular flow but only slightly modify the large elliptic flow of gluons created from the initial state [228]. Although this investigation only focused on the flow of anisotropy of gluons, the obtained large value of v_2 and v_3 indicates that such pre-equilibrium dynamics should be combined with the model calculations of the final-state interactions, such as hydrodynamics or the Boltzmann simulations.

The flow signals in the p–Pb collisions have also been investigated within the framework of the multiphase transport model (AMPT) [206–210]. With a tuned cross sections within the allowed range, $\sigma \sim 1.5 - 3$ mb, AMPT nicely fit the two-particle correlations and the extracted v_2 and v_3 coefficients in high-energy p–Pb collisions [206, 207]. References [206, 210] have shown that AMPT generates a mass ordering of v_2 and v_3 for various hadron species with the coalescence process tuning on. It was also surprisingly observed that the collective behavior in AMPT is built up by a small amount of interactions, where each parton undergoes two collisions on average. The escape mechanism proposed in Refs. [210, 229] seems to be responsible for the anisotropy buildup in AMPT but is dramatically different from the traditional flow development picture of hydrodynamics due to the strong interactions.

With an assumption that the high-energy p–Pb collisions do not reach the threshold to create the QGP but only produce pure hadronic systems, Ref. [211] systematically investigated the 2- and 4-particle correlations of all charged and identified hadrons, using the hadron cascade model Ultra-relativistic Quantum Molecular Dynamics (UrQMD) [127, 128, 230]. Figure 14 shows the two- and four-particle cumulants $c_2\{2\}$ and $c_2\{4\}$ of all charged hadrons, calculated from UrQMD and measured from ALICE. In general, $c_2\{2\}$ decreases with the increase of the pseudo-rapidity gap, which is in agreement with the expectation of suppressing the non-flow effects with a large pseudo-rapidity gap. However, UrQMD still presents a strong centrality dependence of $c_2\{2\}$ for $|\Delta\eta| > 1.0$, which indicates that the remaining non-flow effects are still strong there. In Fig. 14 (right), the $c_2\{4\}$ from the ALICE exhibits there is a transition from positive to negative values, which

indicates the creation of flow-dominated systems for the high-multiplicity events. In contrast, $c_2\{4\}$ from the UrQMD simulations keeps positive for all multiplicity classes, which illustrates that the p–Pb systems created by UrQMD are non-flow dominated.

However, the generally believed collective expansion feature, the mass ordering of $v_2(p_T)$, is reproduced in the UrQMD simulations. Figure 15 shows that these high-multiplicity events from UrQMD present a clear v_2 mass ordering among pions, kaons, and protons, which are qualitatively in agreement with the corresponding ALICE measurement [46]. In UrQMD, the meson–baryon (M–B) cross sections from AQM are about 50% larger than the meson–meson (M–M) ones, which leads to the v_2 splitting between mesons and baryons in the UrQMD simulations. Figure 15 also shows that, after switching off the M–B and M–M interaction channels, the characteristic feature of the v_2 mass ordering disappears. Therefore, even without enough flow generation, the hadronic interactions still lead to a v_2 mass-ordering feature for a hadronic p–Pb system.

In Ref. [231], the created p–Pb systems are described by non-interacting free-streaming particles, followed by a harmonization procedure and a hadronic cascade evolution. Such non-hydrodynamic simulations showed that, although the elliptic flow is under-predicted, the triangular and quadrupolar flow are raised by the free-streaming evolution, which are comparable to the ones obtained from the hydrodynamic simulations. Meanwhile, the v_n mass orderings among pions, kaons, and protons have also been observed in such non-hydrodynamic p–Pb systems due to the hadronic interactions during the late evolution.

6.2 p–p collisions at $\sqrt{s_{NN}} = 7$ TeV and 13 TeV

Like the case for high-energy p–Pb collisions, the long-range two-particle azimuthal correlations with a large pseudo-rapidity separation have also been observed in high-multiplicity p–p collisions at the LHC. This provides new insights for the novel dynamics of the small QCD systems [55–59]. For p–Pb collisions at $\sqrt{s_{NN}} = 5.02$ TeV, the extensive measurements of the 2-particle and multi-particle correlations, extracted flow harmonics for all charged and identified hadrons, as well as the supportive hydrodynamic calculations, strongly indicates that collective expansion has been developed in the small p–Pb systems. However, for high-energy p–p collisions at the LHC, the nature of the observed long-range correlation is still an open question (For different theoretical interpretations, please refer to Refs. [51, 54, 60, 197, 200, 232–237]).

Recently, the ATLAS Collaboration has measured the Fourier coefficients, v_n , in p–p collisions at $\sqrt{s_{NN}} = 13$ TeV, using the two-particle correlations as a function of the

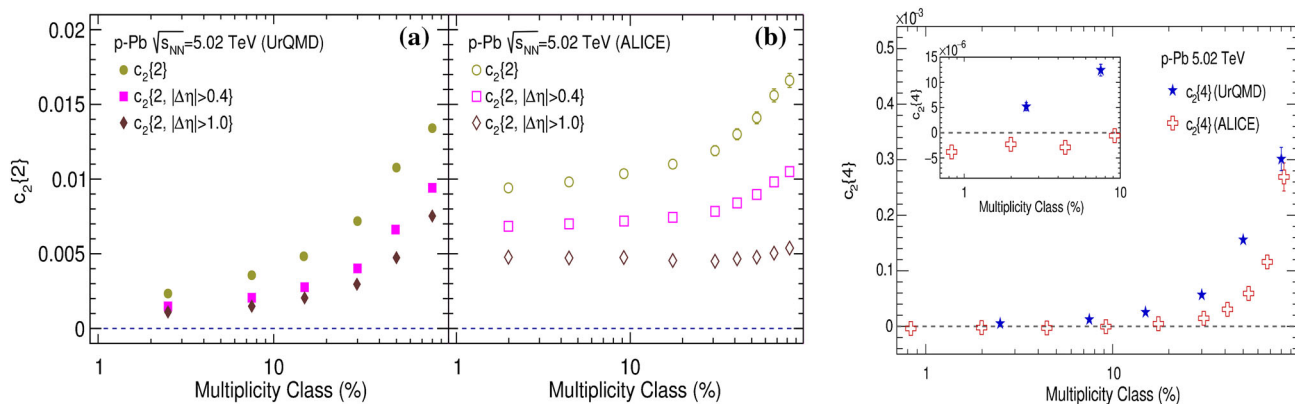
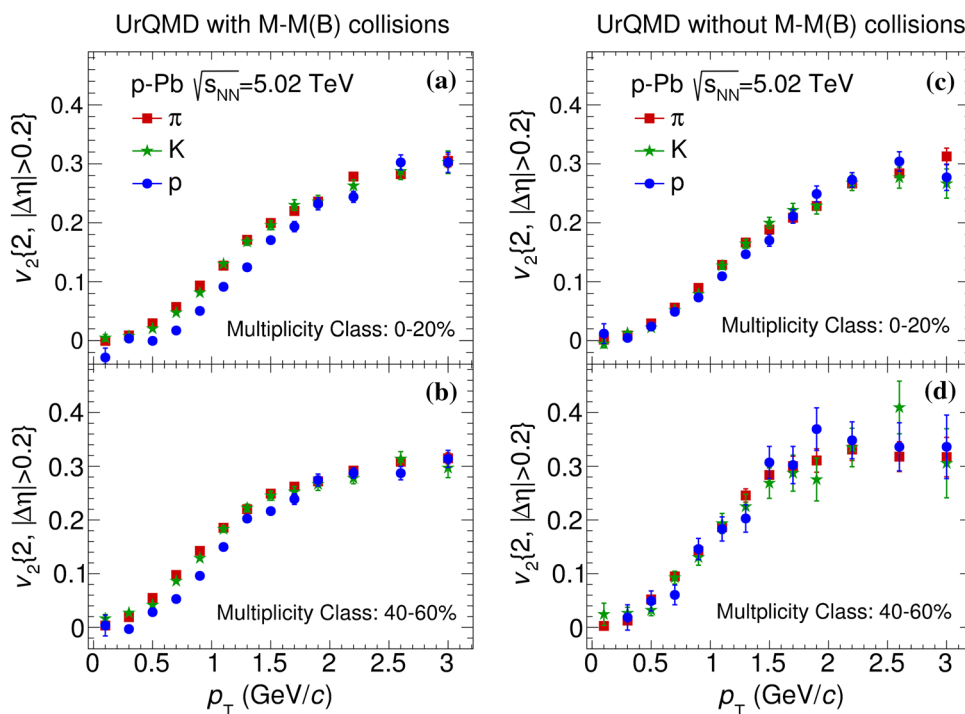


Fig. 14 (Color online) Centrality dependence of $c_2\{2\}$ (left) and $c_2\{4\}$ (right) calculated from UrQMD [211] and measured by ALICE [45]

Fig. 15 (Color online) $v_2(p_T)$ of pions, kaons, and protons in p–Pb collisions at $\sqrt{s_{NN}} = 5.02$ TeV calculated from UrQMD with and without M–M and M–B collisions [211]



relative azimuthal angle and pseudo-rapidity [57]. It was found that the extracted v_2 is approximately a constant as a function of multiplicity and its p_T dependence is very similar to the one measured in the p–Pb and Pb–Pb collisions [57]. The CMS collaboration further measured the v_n coefficients for all charged hadrons, as well as for K_S^0 and $\Lambda/\bar{\Lambda}$ in p–p collisions at $\sqrt{s_{NN}} = 5, 7,$ and 13 TeV, which observed a clear v_2 mass ordering among all charged hadrons, K_S^0 and $\Lambda/\bar{\Lambda}$ [59]. Furthermore, the CMS collaboration has measured the multi-particle cumulants, the key observable to probe the anisotropic collectivity. A negative sign of $c_2\{4\}$ and a positive sign of $c_2\{6\}$ appeared in the high-multiplicity p–p collisions at $\sqrt{s_{NN}} = 13$ TeV [59], which seems to indicate the development of

anisotropic collectivity in high-energy p–p collisions. However, the ATLAS Collaboration reported in Hard Probe 2016 conference that the multiplicity fluctuations could significantly bias the measurements of multi-particle cumulants [238], which indicates that non-flow might mimic the flow signal by pushing the $c_2\{4\}$ to negative values. In order to avoid the bias from multiplicity fluctuations, the so-called “Method 1”, which using the same multiplicity selection for the calculations of cumulants and N_{trk} , is applied. The obtained $c_2\{4\}$, which is less affected by multiplicity fluctuations, does not show negative sign for the multiplicity regions where negative values of $c_2\{4\}$ was reported by CMS.

For small systems, it is also very important to address and evaluate the non-flow effects. Generally, the multi-

particle cumulants, e.g., $c_2\{4\}$, are able to suppress the non-flow of two-particle correlations in traditional Au+Au or Pb+Pb collisions. However, the non-flow contributions to the multi-particle correlations are still remained and might play a non-negligible role in the small p–p collision systems. Recently, the ALICE and ATLAS Collaborations have proposed new 4-particle cumulant methods with $|\Delta\eta|$ gap separation, using 2 or 3 sub-events [239, 240]. By selecting particles from different regions separated by a $|\Delta\eta|$ gap, it is possible to further suppress the non-flow contributions in the multi-particle cumulants. This has been verified in the PYTHIA simulations [241]. The preliminary measurements in p–p collisions at 13 TeV, reported in QM2017 [239, 240], have shown that the non-flow effects are suppressed with these new 4-particle cumulant methods. A negative sign of the 4-particle cumulant was observed by ATLAS collaboration after implementing the 3 sub-event method, while ALICE has not confirm the negative sign of $c_2\{4\}$ with a $|\Delta\eta|$ gap separation due to the limited statistics and relatively smaller acceptance.

Besides the multi-particle cumulants for single flow harmonics, the CMS Collaboration also measured the symmetric cumulants SC(m,n) and normalized symmetric cumulants NSC(m,n) in p–p, p–Pb, and Pb–Pb collisions [242]. It was found that the normalized NSC(3,2) are similar in p–Pb and Pb–Pb collisions, indicating that these two systems present similar initial-state fluctuation patterns for the correlations between ε_2 and ε_3 , while the normalized NSC(4,2) shows certain orderings for the p–p, p–Pb, and Pb–Pb collision systems, which may associates with the different nonlinear response and non-flow effects between the large and small systems.

In short, these recent measurements in p–p collisions $\sqrt{s_{NN}} = 13$ TeV are aimed to evaluate whether or not collective flow has been created in high-multiplicity p–p collisions. Future investigations, from both experimental and theoretical sides, are very crucial to further address this question and for a deep understanding of the underline physics in the small collision systems.

7 Summary

In this paper, we briefly reviewed the collective flow and hydrodynamics in large and small systems at the LHC. One of the important messages we would like to convey to readers is that hydrodynamics and hybrid models are important and useful tools to study various flow observables in high-energy nucleus–nucleus and nucleus–nucleon collisions. With a properly chosen initial condition and well-tuned QGP transport coefficients, hydrodynamics and hybrid models can quantitatively describe the flow

harmonics coefficients, v_n , of all charged hadrons and make very nice predictions for the flow data of identified hadrons. The massive data fitting of the flow harmonics and other related soft hadron data, using the sophisticated hybrid model simulations, have extracted the functions of the temperature-dependent QGP shear and bulk viscosities at the LHC, which demonstrated that the created QGP is an almost perfect fluid with very small shear viscosity close to the KSS bound.

For some flow observables in the high-energy Pb–Pb collisions, e.g., the event-plane correlations, the correlations between different flow harmonics, hydrodynamic and hybrid models can qualitatively, but not quantitatively, describe the data. However, such qualitatively descriptions can still be considered as a success of the hydrodynamics, considering that the initial-state fluctuations contain different intrinsic patterns from the ones extracted from the final-state correlations. The succeeding hydrodynamic evolution drastically changes some of these initial-state correlations, even the signs, making a quantitatively description of the data. On the other hand, these flow data are more sensitive to the details of theoretical model calculations. A further study of these flow observables could reveal more information on the initial-state fluctuations, nonlinear hydrodynamic response, etc., which could also help us to further constrain the initial-state models and to precisely extract the QGP transport coefficients in the future.

As a hot research topic, the flow-like signals in high-energy p–Pb and p–p collisions at the LHC have been widely investigated in both experiment and theory. For the high-multiplicity p–Pb collisions, the observation of the changing signs of the 4 particle cumulants, the v_2 mass orderings, and the supportive calculations from hydrodynamics, strongly indicated the development of collective expansion in the small p–Pb systems. For the high-energy p–p collisions, some similar results, but with smaller magnitudes, have been observed for many flow-like observables. Although these measurements may also be associated with the collective expansion, more detailed investigations are still needed to further understand of the physics in the small p–p systems.

References

1. T.D. Lee, G.C. Wick, Vacuum stability and vacuum excitation in a spin 0 field theory. *Phys. Rev. D* **9**, 2291–2316 (1974). doi:[10.1103/PhysRevD.9.2291](https://doi.org/10.1103/PhysRevD.9.2291)
2. J.C. Collins, M.J. Perry, Superdense matter: neutrons or asymptotically free quarks? *Phys. Rev. Lett.* **34**, 1353 (1975). doi:[10.1103/PhysRevLett.34.1353](https://doi.org/10.1103/PhysRevLett.34.1353)
3. H.G. Baumgardt, J.U. Schott, Y. Sakamoto et al., Shock waves and MACH cones in fast nucleus–nucleus collisions. *Z. Phys. A* **273**, 359–371 (1975). doi:[10.1007/BF01435578](https://doi.org/10.1007/BF01435578)

4. I. Arsene, I.G. Bearden, D. Beavis et al., Quark gluon plasma and color glass condensate at RHIC? The perspective from the BRAHMS experiment. *Nucl. Phys. A* **757**, 1–27 (2005). doi:[10.1016/j.nuclphysa.2005.02.130](https://doi.org/10.1016/j.nuclphysa.2005.02.130)
5. B.B. Back, M.D. Baker, M. Ballintijn et al., The PHOBOS perspective on discoveries at RHIC. *Nucl. Phys. A* **757**, 28–101 (2005). doi:[10.1016/j.nuclphysa.2005.03.084](https://doi.org/10.1016/j.nuclphysa.2005.03.084)
6. J. Adams, M.M. Aggarwal, Z. Ahammed et al., Experimental and theoretical challenges in the search for the quark gluon plasma: the STAR Collaboration's critical assessment of the evidence from RHIC collisions. *Nucl. Phys. A* **757**, 102–183 (2005). doi:[10.1016/j.nuclphysa.2005.03.085](https://doi.org/10.1016/j.nuclphysa.2005.03.085)
7. K. Adcox, S.S. Adler, S. Afanasiev et al., Formation of dense partonic matter in relativistic nucleus–nucleus collisions at RHIC: experimental evaluation by the PHENIX collaboration. *Nucl. Phys. A* **757**, 184–283 (2005). doi:[10.1016/j.nuclphysa.2005.03.086](https://doi.org/10.1016/j.nuclphysa.2005.03.086)
8. M. Gyulassy, The QGP discovered at RHIC (2004), [arXiv: nucl-th/0403032](https://arxiv.org/abs/nucl-th/0403032)
9. B. Muller, J.L. Nagle, Results from the relativistic heavy ion collider. *Annu. Rev. Nucl. Part. Sci.* **56**, 93–135 (2006). doi:[10.1146/annurev.nucl.56.080805.140556](https://doi.org/10.1146/annurev.nucl.56.080805.140556)
10. P.F. Kolb, U.W. Heinz, Hydrodynamic description of ultrarelativistic heavy ion collisions (2003), [arXiv: nucl-th/0305084](https://arxiv.org/abs/nucl-th/0305084)
11. B. Alver, B.B. Back, M.D. Baker et al., System size, energy, pseudorapidity, and centrality dependence of elliptic flow. *Phys. Rev. Lett.* **98**, 242302 (2007). doi:[10.1103/PhysRevLett.98.242302](https://doi.org/10.1103/PhysRevLett.98.242302)
12. M. Miller, R. Snellings, Eccentricity fluctuations and its possible effect on elliptic flow measurements (2003), [arXiv: nucl-ex/0312008](https://arxiv.org/abs/nucl-ex/0312008)
13. B. Alver, B.B. Back, M.D. Baker et al., Importance of correlations and fluctuations on the initial source eccentricity in high-energy nucleus–nucleus collisions. *Phys. Rev. C* **77**, 014906 (2008). doi:[10.1103/PhysRevC.77.014906](https://doi.org/10.1103/PhysRevC.77.014906)
14. J.Y. Ollitrault, Anisotropy as a signature of transverse collective flow. *Phys. Rev. D* **46**, 229–245 (1992). doi:[10.1103/PhysRevD.46.229](https://doi.org/10.1103/PhysRevD.46.229)
15. S. Voloshin, Y. Zhang, Flow study in relativistic nuclear collisions by Fourier expansion of azimuthal particle distributions. *Z. Phys. C* **70**, 665–672 (1996). doi:[10.1007/s002880050141](https://doi.org/10.1007/s002880050141)
16. S.A. Voloshin, A.M. Poskanzer, R. Snellings, Collective phenomena in non-central nuclear collisions (2008), [arXiv: 0809.2949](https://arxiv.org/abs/0809.2949)
17. R. Snellings, Elliptic flow: a brief review. *New J. Phys.* **13**, 055008 (2011). doi:[10.1088/1367-2630/13/5/055008](https://doi.org/10.1088/1367-2630/13/5/055008)
18. U. Heinz, R. Snellings, Collective flow and viscosity in relativistic heavy-ion collisions. *Annu. Rev. Nucl. Part. Sci.* **63**, 123–151 (2013). doi:[10.1146/annurev-nucl-102212-170540](https://doi.org/10.1146/annurev-nucl-102212-170540)
19. C. Gale, S. Jeon, B. Schenke, Hydrodynamic modeling of heavy-ion collisions. *Int. J. Mod. Phys. A* **28**, 1340011 (2013). doi:[10.1142/S0217751X13400113](https://doi.org/10.1142/S0217751X13400113)
20. H.C. Song, Hydrodynamic modelling for relativistic heavy-ion collisions at RHIC and LHC. *Pramana* **84**, 703–715 (2015). doi:[10.1007/s12043-015-0971-2](https://doi.org/10.1007/s12043-015-0971-2)
21. M. Luzum, H. Petersen, Initial state fluctuations and final state correlations in relativistic heavy-ion collisions. *J. Phys. G* **41**, 063102 (2014). doi:[10.1088/0954-3899/41/6/063102](https://doi.org/10.1088/0954-3899/41/6/063102)
22. J.Y. Jia, Event-shape fluctuations and flow correlations in ultra-relativistic heavy-ion collisions. *J. Phys. G* **41**, 124003 (2014). doi:[10.1088/0954-3899/41/12/124003](https://doi.org/10.1088/0954-3899/41/12/124003)
23. B.H. Alver, C. Gombeaud, M. Luzum et al., Triangular flow in hydrodynamics and transport theory. *Phys. Rev. C* **82**, 034913 (2010). doi:[10.1103/PhysRevC.82.034913](https://doi.org/10.1103/PhysRevC.82.034913)
24. K. Aamodt, B. Abelev, A. Abrahantes et al., Higher harmonic anisotropic flow measurements of charged particles in Pb–Pb collisions at $\sqrt{s_{NN}} = 2.76$ TeV. *Phys. Rev. Lett.* **107**, 03230 (2011). doi:[10.1103/PhysRevLett.107.032301](https://doi.org/10.1103/PhysRevLett.107.032301)
25. F.G. Gardim, F. Grassi, M. Luzum et al., Mapping the hydrodynamic response to the initial geometry in heavy-ion collisions. *Phys. Rev. C* **85**, 024908 (2012). doi:[10.1103/PhysRevC.85.024908](https://doi.org/10.1103/PhysRevC.85.024908)
26. G. Aad, H.M. Gray, Z. Marshall, Measurement of the azimuthal anisotropy for charged particle production in $\sqrt{s_{NN}} = 2.76$ TeV lead-lead collisions with the ATLAS detector. *Phys. Rev. C* **86**, 014907 (2012). doi:[10.1103/PhysRevC.86.014907](https://doi.org/10.1103/PhysRevC.86.014907)
27. M. Luzum, J.Y. Ollitrault, Extracting the shear viscosity of the quark–gluon plasma from flow in ultra-central heavy-ion collisions. *Nucl. Phys. A* **904–905**, 377c–380c (2013). doi:[10.1016/j.nuclphysa.2013.02.028](https://doi.org/10.1016/j.nuclphysa.2013.02.028)
28. A. Rizzi, R. Erbacher, Y. Weng, Studies of azimuthal dihadron correlations in ultra-central PbPb collisions at $\sqrt{s_{NN}} = 2.76$ TeV. *JHEP* **02**, 088 (2014). doi:[10.1007/JHEP02\(2014\)088](https://doi.org/10.1007/JHEP02(2014)088)
29. G. Aad, M. Barbero, C.P. Bee, Measurement of the distributions of event-by-event flow harmonics in lead–lead collisions at $\sqrt{s_{NN}} = 2.76$ TeV with the ATLAS detector at the LHC. *JHEP* **11**, 183 (2013). doi:[10.1007/JHEP11\(2013\)183](https://doi.org/10.1007/JHEP11(2013)183)
30. C. Gale, S.Y. Jeon, B. Schenke et al., Event-by-event anisotropic flow in heavy-ion collisions from combined Yang–Mills and viscous fluid dynamics. *Phys. Rev. Lett.* **110**, 012302 (2013). doi:[10.1103/PhysRevLett.110.012302](https://doi.org/10.1103/PhysRevLett.110.012302)
31. G. Aad, B. Abbott, J. Abdallah et al., Measurement of event-plane correlations in $\sqrt{s_{NN}} = 2.76$ TeV lead-lead collisions with the ATLAS detector. *Phys. Rev. C* **90**, 024905 (2014). doi:[10.1103/PhysRevC.90.024905](https://doi.org/10.1103/PhysRevC.90.024905)
32. Z. Qiu, U. Heinz, Hydrodynamic event-plane correlations in Pb+Pb collisions at $\sqrt{s} = 2.76$ ATeV. *Phys. Lett. B* **717**, 261–265 (2012). doi:[10.1016/j.physletb.2012.09.030](https://doi.org/10.1016/j.physletb.2012.09.030)
33. G. Aad, B. Abbott, J. Abdallah et al., Measurement of the correlation between flow harmonics of different order in lead–lead collisions at $\sqrt{s_{NN}} = 2.76$ TeV with the ATLAS detector. *Phys. Rev. C* **92**, 034903 (2015). doi:[10.1103/PhysRevC.92.034903](https://doi.org/10.1103/PhysRevC.92.034903)
34. J. Adam, D. Adamová, M.M. Aggarwal et al., Correlated event-by-event fluctuations of flow harmonics in Pb–Pb collisions at $\sqrt{s_{NN}} = 2.76$ TeV (2016), [arXiv: 1604.07663](https://arxiv.org/abs/1604.07663)
35. G. Giacalone, L. Yan, J. Noronha-Hostler et al., Symmetric cumulants and event-plane correlations in Pb + Pb collisions. *Phys. Rev. C* **94**, 014906 (2016). doi:[10.1103/PhysRevC.94.014906](https://doi.org/10.1103/PhysRevC.94.014906)
36. X.R. Zhu, Y. Zhou, H.J. Xu et al., Correlations of flow harmonics in 2.76 A TeV Pb–Pb collisions (2016), [arXiv: 1608.05305](https://arxiv.org/abs/1608.05305)
37. J. Qian, U. Heinz, Hydrodynamic flow amplitude correlations in event-by-event fluctuating heavy-ion collisions. *Phys. Rev. C* **94**, 024910 (2016). doi:[10.1103/PhysRevC.94.024910](https://doi.org/10.1103/PhysRevC.94.024910)
38. U. Heinz, Z. Qiu, C. Shen, Fluctuating flow angles and anisotropic flow measurements. *Phys. Rev. C* **87**, 034913 (2013). doi:[10.1103/PhysRevC.87.034913](https://doi.org/10.1103/PhysRevC.87.034913)
39. F.G. Gardim, F. Grassi, M. Luzum et al., Breaking of factorization of two-particle correlations in hydrodynamics. *Phys. Rev. C* **87**, 031901 (2013). doi:[10.1103/PhysRevC.87.031901](https://doi.org/10.1103/PhysRevC.87.031901)
40. V. Khachatryan, A.M. Sirunyan, A. Tumasyan et al., Evidence for transverse momentum and pseudorapidity dependent event plane fluctuations in PbPb and pPb collisions. *Phys. Rev. C* **92**, 034911 (2015). doi:[10.1103/PhysRevC.92.034911](https://doi.org/10.1103/PhysRevC.92.034911)
41. S. chatrchyan, V. Khachatryan, A.M. Sirunyan, Observation of long-range near-side angular correlations in proton–lead collisions at the LHC. *Phys. Lett. B* **718**, 795–814 (2013). doi:[10.1016/j.physletb.2012.11.025](https://doi.org/10.1016/j.physletb.2012.11.025)
42. B. Abelev, J. Adam, D. Adamova, et al., Long-range angular correlations on the near and away side in p–Pb collisions at

- $\sqrt{s_{NN}} = 5.02$ TeV. Phys. Lett. B **719**, 29–41 (2013). doi:[10.1016/j.physletb.2013.01.012](https://doi.org/10.1016/j.physletb.2013.01.012)
43. G. Aad, T. Abajyan, B. Abbott et al., Measurement with the ATLAS detector of multi-particle azimuthal correlations in p+Pb collisions at $\sqrt{s_{NN}} = 5.02$ TeV. Phys. Lett. B **725**, 60–78 (2013). doi:[10.1016/j.physletb.2013.06.057](https://doi.org/10.1016/j.physletb.2013.06.057)
 44. V. Khachatryan, A.M. Sirunyan, A. Tumasyan et al., Evidence for collective multiparticle correlations in p–Pb collisions. Phys. Rev. Lett. **115**, 012301 (2015). doi:[10.1103/PhysRevLett.115.012301](https://doi.org/10.1103/PhysRevLett.115.012301)
 45. B. Abelev, J. Adam, D. Adamova et al., Long-range angular correlations on the near and away side in p–Pb collisions at $\sqrt{s_{NN}} = 5.02$ TeV. Phys. Rev. C **90**, 054901 (2014). doi:[10.1103/PhysRevC.90.054901](https://doi.org/10.1103/PhysRevC.90.054901)
 46. V. Khachatryan, A.M. Sirunyan, A. Tumasyan et al., Long-range angular correlations of π , K and p in p–Pb collisions at $\sqrt{s_{NN}} = 5.02$ TeV. Phys. Lett. B **726**, 164–177 (2013). doi:[10.1016/j.physletb.2013.08.024](https://doi.org/10.1016/j.physletb.2013.08.024)
 47. V. Khachatryan, A.M. Sirunyan, A. Tumasyan et al., Long-range two-particle correlations of strange hadrons with charged particles in pPb and PbPb collisions at LHC energies. Phys. Lett. B **742**, 200–224 (2015). doi:[10.1016/j.physletb.2015.01.034](https://doi.org/10.1016/j.physletb.2015.01.034)
 48. P. Bozek, Collective flow in p–Pb and d–Pd collisions at TeV energies. Phys. Rev. C **85**, 014911 (2012). doi:[10.1103/PhysRevC.85.014911](https://doi.org/10.1103/PhysRevC.85.014911)
 49. P. Bozek, W. Broniowski, Correlations from hydrodynamic flow in p–Pb collisions. Phys. Lett. B **718**, 1557–1561 (2013). doi:[10.1016/j.physletb.2012.12.051](https://doi.org/10.1016/j.physletb.2012.12.051)
 50. P. Bozek, W. Broniowski, G. Torrieri, Mass hierarchy in identified particle distributions in proton–lead collisions. Phys. Rev. Lett. **111**, 172303 (2013). doi:[10.1103/PhysRevLett.111.172303](https://doi.org/10.1103/PhysRevLett.111.172303)
 51. A. Bzdak, B. Schenke, P. Tribedy et al., Initial state geometry and the role of hydrodynamics in proton–proton, proton–nucleus and deuteron–nucleus collisions. Phys. Rev. C **87**, 064906 (2013). doi:[10.1103/PhysRevC.87.064906](https://doi.org/10.1103/PhysRevC.87.064906)
 52. G.Y. Qin, B. Müller, Elliptic and triangular flow anisotropy in deuteron–gold collisions at $\sqrt{s_{NN}} = 200$ GeV at RHIC and in proton–lead collisions at $\sqrt{s_{NN}} = 5.02$ TeV at the LHC. Phys. Rev. C **89**, 044902 (2014). doi:[10.1103/PhysRevC.89.044902](https://doi.org/10.1103/PhysRevC.89.044902)
 53. K. Werner, M. Bleicher, B. Guiot et al., Evidence for flow from hydrodynamic simulations of p–Pb collisions at 5.02 TeV from v_2 mass splitting. Phys. Rev. Lett. **112**, 232301 (2014). doi:[10.1103/PhysRevLett.112.232301](https://doi.org/10.1103/PhysRevLett.112.232301)
 54. B. Schenke, R. Venugopalan, Eccentric protons? Sensitivity of flow to system size and shape in p+p, p+Pb and Pb+Pb collisions. Phys. Rev. Lett. **113**, 102301 (2014). doi:[10.1103/PhysRevLett.113.102301](https://doi.org/10.1103/PhysRevLett.113.102301)
 55. S. Chatrchyan, V. Khachatryan, A.M. Sirunyan et al., Observation of long-range near-side angular correlations in proton–proton collisions at the LHC. JHEP **09**, 091 (2010). doi:[10.1007/JHEP09\(2010\)091](https://doi.org/10.1007/JHEP09(2010)091)
 56. W. Li, Observation of a ‘Ridge’ correlation structure in high multiplicity proton–proton collisions: a brief review. Mod. Phys. Lett. A **27**, 1230018 (2012). doi:[10.1142/S0217732312300182](https://doi.org/10.1142/S0217732312300182)
 57. G. Aad, B. Abbott, J. Abdallah et al., Observation of long-range elliptic azimuthal anisotropies in $\sqrt{s} = 13$ and 2.76 TeV pp collisions with the ATLAS detector. Phys. Rev. Lett. **116**, 172301 (2016). doi:[10.1103/PhysRevLett.116.172301](https://doi.org/10.1103/PhysRevLett.116.172301)
 58. V. Khachatryan, A.M. Sirunyan, A. Tumasyan et al., Measurement of long-range near-side two-particle angular correlations in pp collisions at $\sqrt{s} = 13$ TeV. Phys. Rev. Lett. **116**, 172302 (2016). doi:[10.1103/PhysRevLett.116.172302](https://doi.org/10.1103/PhysRevLett.116.172302)
 59. V. Khachatryan, A.M. Sirunyan, A. Tumasyan et al., Evidence for collectivity in pp collisions at the LHC (2016), [arXiv: 1606.06198](https://arxiv.org/abs/1606.06198)
 60. K. Dusling, W. Li, B. Schenke, Novel collective phenomena in high-energy proton–proton and proton–nucleus collisions. Int. J. Mod. Phys. E **25**, 1630002 (2016). doi:[10.1142/S0218301316300022](https://doi.org/10.1142/S0218301316300022)
 61. D.A. Teaney, Viscous hydrodynamics and the quark gluon plasma (2009), [arXiv: nucl-th/0905.2433](https://arxiv.org/abs/nucl-th/0905.2433)
 62. P. Romatschke, New developments in relativistic viscous hydrodynamics. Int. J. Mod. Phys. E **19**, 1–53 (2010). doi:[10.1142/S0218301310014613](https://doi.org/10.1142/S0218301310014613)
 63. P. Huovinen, Hydrodynamics at RHIC and LHC: what have we learned? Int. J. Mod. Phys. E **22**, 1330029 (2013). doi:[10.1142/S0218301313300294](https://doi.org/10.1142/S0218301313300294)
 64. P. Romatschke, U. Romatschke, Viscosity information from relativistic nuclear collisions: how perfect is the fluid observed at RHIC? Phys. Rev. Lett. **99**, 172301 (2007). doi:[10.1103/PhysRevLett.99.172301](https://doi.org/10.1103/PhysRevLett.99.172301)
 65. M. Luzum, P. Romatschke, Conformal relativistic viscous hydrodynamics: applications to RHIC results at $s(NN)^{1/2} = 200$ -GeV. Phys. Rev. C **78**, 034915 (2008). doi:[10.1103/PhysRevC.78.034915](https://doi.org/10.1103/PhysRevC.78.034915)
 66. H.C. Song, U.W. Heinz, Suppression of elliptic flow in a minimally viscous quark–gluon plasma. Phys. Lett. B **658**, 279–283 (2008). doi:[10.1016/j.physletb.2007.11.019](https://doi.org/10.1016/j.physletb.2007.11.019)
 67. H.C. Song, U.W. Heinz, Causal viscous hydrodynamics in 2+1 dimensions for relativistic heavy-ion collisions. Phys. Rev. C **77**, 064901 (2008). doi:[10.1103/PhysRevC.77.064901](https://doi.org/10.1103/PhysRevC.77.064901)
 68. H.C. Song, Causal viscous hydrodynamics for relativistic heavy ion collisions, Ph.D. thesis, Ohio State U, 2009, <http://inspirehep.net/record/829461/files/arXiv:0908.3656.pdf>, [arXiv: 0908.3656](https://arxiv.org/abs/0908.3656)
 69. K. Dusling, D. Teaney, Simulating elliptic flow with viscous hydrodynamics. Phys. Rev. C **77**, 034905 (2008). doi:[10.1103/PhysRevC.77.034905](https://doi.org/10.1103/PhysRevC.77.034905)
 70. D. Molnar, P. Huovinen, Dissipative effects from transport and viscous hydrodynamics. J. Phys. G **35**, 104125 (2008). doi:[10.1088/0954-3899/35/10/104125](https://doi.org/10.1088/0954-3899/35/10/104125)
 71. P. Bozek, Bulk and shear viscosities of matter created in relativistic heavy-ion collisions. Phys. Rev. C **81**, 034909 (2010). doi:[10.1103/PhysRevC.81.034909](https://doi.org/10.1103/PhysRevC.81.034909)
 72. A.K. Chaudhuri, Centrality dependence of elliptic flow and QGP viscosity. J. Phys. G **37**, 075011 (2010). doi:[10.1088/0954-3899/37/7/075011](https://doi.org/10.1088/0954-3899/37/7/075011)
 73. B. Schenke, S. Jeon, C. Gale, Elliptic and triangular flow in event-by-event (3+1)D viscous hydrodynamics. Phys. Rev. Lett. **106**, 042301 (2011). doi:[10.1103/PhysRevLett.106.042301](https://doi.org/10.1103/PhysRevLett.106.042301)
 74. W. Israel, Nonstationary irreversible thermodynamics: a causal relativistic theory. Ann. Phys. **100**, 310–331 (1976). doi:[10.1016/0003-4916\(76\)90064-6](https://doi.org/10.1016/0003-4916(76)90064-6)
 75. A. Muronga, D.H. Rischke, Evolution of hot, dissipative quark matter in relativistic nuclear collisions (2004), [arXiv: nucl-th/0407114](https://arxiv.org/abs/nucl-th/0407114)
 76. R. Baier, P. Romatschke, U.A. Wiedemann, Dissipative hydrodynamics and heavy ion collisions. Phys. Rev. C **73**, 064903 (2006). doi:[10.1103/PhysRevC.73.064903](https://doi.org/10.1103/PhysRevC.73.064903)
 77. R. Baier, P. Romatschke, D.T. Son et al., Relativistic viscous hydrodynamics, conformal invariance, and holography. JHEP **04**, 100 (2008). doi:[10.1088/1126-6708/2008/04/100](https://doi.org/10.1088/1126-6708/2008/04/100)
 78. B. Betz, D. Henkel, D.H. Rischke, From kinetic theory to dissipative fluid dynamics. Prog. Part. Nucl. Phys. **62**, 556–561 (2009). doi:[10.1016/j.pnpnp.2008.12.018](https://doi.org/10.1016/j.pnpnp.2008.12.018)
 79. G.S. Denicol, H. Niemi, E. Molnar et al., Derivation of transient relativistic fluid dynamics from the Boltzmann equation. Phys. Rev. D **85**, 114047 (2012). doi:[10.1103/PhysRevD.85.114047](https://doi.org/10.1103/PhysRevD.85.114047)
 80. G.S. Denicol, E. Molnar, H. Niemi et al., Derivation of fluid dynamics from kinetic theory with the 14-moment

- approximation. *Eur. Phys. J. A* **48**, 170 (2012). doi:[10.1140/epja/i2012-12170-x](https://doi.org/10.1140/epja/i2012-12170-x)
81. M. Martinez, M. Strickland, Dissipative dynamics of highly anisotropic systems. *Nucl. Phys. A* **848**, 183–197 (2010). doi:[10.1016/j.nuclphysa.2010.08.011](https://doi.org/10.1016/j.nuclphysa.2010.08.011)
 82. W. Florkowski, R. Ryblewski, Highly-anisotropic and strongly-dissipative hydrodynamics for early stages of relativistic heavy-ion collisions. *Phys. Rev. C* **83**, 034907 (2011). doi:[10.1103/PhysRevC.83.034907](https://doi.org/10.1103/PhysRevC.83.034907)
 83. S. Jeon, U. Heinz, Introduction to hydrodynamics, in *Quark–Gluon Plasma 5*, edited by X.-N. Wang (2016) pp. 131–187. doi:[10.1142/9789814663717_0003](https://doi.org/10.1142/9789814663717_0003)
 84. M.A. Stephanov, Non-Gaussian fluctuations near the QCD critical point. *Phys. Rev. Lett.* **102**, 032301 (2009). doi:[10.1103/PhysRevLett.102.032301](https://doi.org/10.1103/PhysRevLett.102.032301)
 85. M.A. Stephanov, On the sign of kurtosis near the QCD critical point. *Phys. Rev. Lett.* **107**, 052301 (2011). doi:[10.1103/PhysRevLett.107.052301](https://doi.org/10.1103/PhysRevLett.107.052301)
 86. L.J. Jiang, P.F. Li, H.C. Song, Correlated fluctuations near the QCD critical point. *Phys. Rev. C* **94**, 024918 (2016). doi:[10.1103/PhysRevC.94.024918](https://doi.org/10.1103/PhysRevC.94.024918)
 87. L.J. Jiang, P.F. Li, H.C. Song, Multiplicity fluctuations of net protons on the hydrodynamic freeze-out surface. *Nucl. Phys. A* **956**, 360–364 (2016). doi:[10.1016/j.nuclphysa.2016.01.034](https://doi.org/10.1016/j.nuclphysa.2016.01.034)
 88. M. Martinez, R. Ryblewski, M. Strickland, Boost-invariant (2+1)-dimensional anisotropic hydrodynamics. *Phys. Rev. C* **85**, 064913 (2012). doi:[10.1103/PhysRevC.85.064913](https://doi.org/10.1103/PhysRevC.85.064913)
 89. W. Florkowski, R. Ryblewski, M. Strickland, Anisotropic hydrodynamics for rapidly expanding systems. *Nucl. Phys. A* **916**, 249–259 (2013). doi:[10.1016/j.nuclphysa.2013.08.004](https://doi.org/10.1016/j.nuclphysa.2013.08.004)
 90. R. Ryblewski, W. Florkowski, Highly-anisotropic hydrodynamics in 3+1 space-time dimensions. *Phys. Rev. C* **85**, 064901 (2012). doi:[10.1103/PhysRevC.85.064901](https://doi.org/10.1103/PhysRevC.85.064901)
 91. D. Bazow, U.W. Heinz, M. Strickland, Second-order (2+1)-dimensional anisotropic hydrodynamics. *Phys. Rev. C* **90**, 054910 (2014). doi:[10.1103/PhysRevC.90.054910](https://doi.org/10.1103/PhysRevC.90.054910)
 92. D. Bazow, U.W. Heinz, M. Martinez, Nonconformal viscous anisotropic hydrodynamics. *Phys. Rev. C* **91**, 064903 (2015). doi:[10.1103/PhysRevC.91.064903](https://doi.org/10.1103/PhysRevC.91.064903)
 93. M. Strickland, Recent progress in anisotropic hydrodynamics 2016, [arXiv: 1611.05056](https://arxiv.org/abs/1611.05056)<http://inspirehep.net/record/1498322/files/arXiv:1611.05056.pdf>
 94. K. Paech, H. Stoecker, A. Dumitru, Hydrodynamics near a chiral critical point. *Phys. Rev. C* **68**, 044907 (2003). doi:[10.1103/PhysRevC.68.044907](https://doi.org/10.1103/PhysRevC.68.044907)
 95. M. Nahrgang, S. Leupold, C. Herold et al., Nonequilibrium chiral fluid dynamics including dissipation and noise. *Phys. Rev. C* **84**, 024912 (2011). doi:[10.1103/PhysRevC.84.024912](https://doi.org/10.1103/PhysRevC.84.024912)
 96. M. Nahrgang, S. Leupold, M. Bleicher, Equilibration and relaxation times at the chiral phase transition including reheating. *Phys. Lett. B* **711**, 109–116 (2012). doi:[10.1016/j.physletb.2012.03.059](https://doi.org/10.1016/j.physletb.2012.03.059)
 97. C. Herold, M. Nahrgang, I. Mishustin et al., Chiral fluid dynamics with explicit propagation of the Polyakov loop. *Phys. Rev. C* **87**, 014907 (2013). doi:[10.1103/PhysRevC.87.014907](https://doi.org/10.1103/PhysRevC.87.014907)
 98. C. Herold, M. Nahrgang, Y. Yan et al., Dynamical net-proton fluctuations near a QCD critical point. *Phys. Rev. C* **93**, 021902 (2016). doi:[10.1103/PhysRevC.93.021902](https://doi.org/10.1103/PhysRevC.93.021902)
 99. G.S. Denicol, H. Niemi, I. Bouras et al., Solving the heat-flow problem with transient relativistic fluid dynamics. *Phys. Rev. D* **89**, 074005 (2014). doi:[10.1103/PhysRevD.89.074005](https://doi.org/10.1103/PhysRevD.89.074005)
 100. P. Huovinen, P. Petreczky, QCD equation of state and hadron resonance gas. *Nucl. Phys. A* **837**, 26–53 (2010). doi:[10.1016/j.nuclphysa.2010.02.015](https://doi.org/10.1016/j.nuclphysa.2010.02.015)
 101. C. Shen, U. Heinz, P. Huovinen et al., Systematic parameter study of hadron spectra and elliptic flow from viscous hydrodynamic simulations of Au+Au collisions at $\sqrt{s_{NN}} = 200$ GeV. *Phys. Rev. C* **82**, 054904 (2010). doi:[10.1103/PhysRevC.82.054904](https://doi.org/10.1103/PhysRevC.82.054904)
 102. P.F. Kolb, J. Sollfrank, U.W. Heinz, Anisotropic transverse flow and the quark hadron phase transition. *Phys. Rev. C* **62**, 054909 (2000). doi:[10.1103/PhysRevC.62.054909](https://doi.org/10.1103/PhysRevC.62.054909)
 103. D. Kharzeev, M. Nardi, Hadron production in nuclear collisions at RHIC and high density QCD. *Phys. Lett. B* **507**, 121–128 (2001). doi:[10.1016/S0370-2693\(01\)00457-9](https://doi.org/10.1016/S0370-2693(01)00457-9)
 104. M.L. Miller, K. Reygers, S.J. Sanders et al., Glauber modeling in high energy nuclear collisions. *Annu. Rev. Nucl. Part. Sci.* **57**, 205–243 (2007). doi:[10.1146/annurev.nucl.57.090506.123020](https://doi.org/10.1146/annurev.nucl.57.090506.123020)
 105. H.-J. Drescher, Y. Nara, Effects of fluctuations on the initial eccentricity from the color glass condensate in heavy ion collisions. *Phys. Rev. C* **75**, 034905 (2007). doi:[10.1103/PhysRevC.75.034905](https://doi.org/10.1103/PhysRevC.75.034905)
 106. T. Hirano, Y. Nara, Eccentricity fluctuation effects on elliptic flow in relativistic heavy ion collisions. *Phys. Rev. C* **79**, 064904 (2009). doi:[10.1103/PhysRevC.79.064904](https://doi.org/10.1103/PhysRevC.79.064904)
 107. R.S. Bhalerao, A. Jaiswal, S. Pal, Collective flow in event-by-event partonic transport plus hydrodynamics hybrid approach. *Phys. Rev. C* **92**, 014903 (2015). doi:[10.1103/PhysRevC.92.014903](https://doi.org/10.1103/PhysRevC.92.014903)
 108. L.G. Pang, Q. Wang, X.N. Wang, Effects of initial flow velocity fluctuation in event-by-event (3+1)D hydrodynamics. *Phys. Rev. C* **86**, 024911 (2012). doi:[10.1103/PhysRevC.86.024911](https://doi.org/10.1103/PhysRevC.86.024911)
 109. H.J. Xu, Z.P. Li, H.C. Song, High-order flow harmonics of identified hadrons in 2.76A TeV Pb + Pb collisions. *Phys. Rev. C* **93**, 064905 (2016). doi:[10.1103/PhysRevC.93.064905](https://doi.org/10.1103/PhysRevC.93.064905)
 110. B. Schenke, P. Tribedy, R. Venugopalan, Event-by-event gluon multiplicity, energy density, and eccentricities in ultrarelativistic heavy-ion collisions. *Phys. Rev. C* **86**, 034908 (2012). doi:[10.1103/PhysRevC.86.034908](https://doi.org/10.1103/PhysRevC.86.034908)
 111. R. Paatelainen, K.J. Eskola, H. Niemi et al., Fluid dynamics with saturated minijet initial conditions in ultrarelativistic heavy-ion collisions. *Phys. Lett. B* **731**, 126–130 (2014). doi:[10.1016/j.physletb.2014.02.018](https://doi.org/10.1016/j.physletb.2014.02.018)
 112. H. Niemi, K.J. Eskola, R. Paatelainen, Event-by-event fluctuations in a perturbative QCD + saturation + hydrodynamics model: determining QCD matter shear viscosity in ultrarelativistic heavy-ion collisions. *Phys. Rev. C* **93**, 024907 (2016). doi:[10.1103/PhysRevC.93.024907](https://doi.org/10.1103/PhysRevC.93.024907)
 113. J.S. Moreland, J.E. Bernhard, S.A. Bass, Alternative ansatz to wounded nucleon and binary collision scaling in high-energy nuclear collisions. *Phys. Rev. C* **92**, 011901 (2015). doi:[10.1103/PhysRevC.92.011901](https://doi.org/10.1103/PhysRevC.92.011901)
 114. J. Liu, C. Shen, U. Heinz, Pre-equilibrium evolution effects on heavy-ion collision observables. *Phys. Rev. C* **91**, 064906 (2015). doi:[10.1103/PhysRevC.92.049904](https://doi.org/10.1103/PhysRevC.92.049904)
 115. K. Werner, Iu Karpenko, T. Pierog, Evidence for hydrodynamic evolution in proton-proton scattering at 900 GeV. *Phys. Rev. C* **83**, 044915 (2011). doi:[10.1103/PhysRevC.83.044915](https://doi.org/10.1103/PhysRevC.83.044915)
 116. H. Petersen, M. Bleicher, Ideal hydrodynamics and elliptic flow at SPS energies: importance of the initial conditions. *Phys. Rev. C* **79**, 054904 (2009). doi:[10.1103/PhysRevC.79.054904](https://doi.org/10.1103/PhysRevC.79.054904)
 117. H. Petersen, J. Steinheimer, G. Burau et al., Elliptic flow in an integrated (3+1)d microscopic + macroscopic approach with fluctuating initial conditions. *Eur. Phys. J. C* **62**, 31–36 (2009). doi:[10.1140/epjc/s10052-009-0921-6](https://doi.org/10.1140/epjc/s10052-009-0921-6)
 118. B. Schenke, S. Schlichting, 3D glasma initial state for relativistic heavy ion collisions. *Phys. Rev. C* **94**, 044907 (2016). doi:[10.1103/PhysRevC.94.044907](https://doi.org/10.1103/PhysRevC.94.044907)
 119. F. Cooper, G. Frye, *Phys. Rev. D* **10**, 186 (1974)
 120. T. Hirano, M. Gyulassy, Perfect fluidity of the quark gluon plasma core as seen through its dissipative hadronic corona. *Nucl. Phys. A* **769**, 71–94 (2006). doi:[10.1016/j.nuclphysa.2006.02.005](https://doi.org/10.1016/j.nuclphysa.2006.02.005)

121. H.C. Song, S.A. Bass, U. Heinz, Viscous QCD matter in a hybrid hydrodynamic+Boltzmann approach. *Phys. Rev. C* **83**, 024912 (2011). doi:[10.1103/PhysRevC.83.024912](https://doi.org/10.1103/PhysRevC.83.024912)
122. S. Ryu, S. Jeon, C. Gale et al., MUSIC with the UrQMD afterburner. *Nucl. Phys. A* **904–905**, 389c–392c (2013). doi:[10.1016/j.nuclphysa.2013.02.031](https://doi.org/10.1016/j.nuclphysa.2013.02.031)
123. Iu A. Karpenko, M. Bleicher, P. Huovinen, 3+1 dimensional viscous hydrodynamics at high baryon densities. *J. Phys. Conf. Ser.* **503**, 012040 (2014). doi:[10.1088/1742-6596/503/1/012040](https://doi.org/10.1088/1742-6596/503/1/012040)
124. H.T. Ding, F. Karsch, S. Mukherjee, Thermodynamics of strong-interaction matter from Lattice QCD. *Int. J. Mod. Phys. E* **24**, 1530007 (2015). doi:[10.1142/S0218301315300076](https://doi.org/10.1142/S0218301315300076)
125. K. Dusling, T. Schäfer, Bulk viscosity, particle spectra and flow in heavy-ion collisions. *Phys. Rev. C* **85**, 044909 (2012). doi:[10.1103/PhysRevC.85.044909](https://doi.org/10.1103/PhysRevC.85.044909)
126. J. Noronha-Hostler, G.S. Denicol, J. Noronha et al., Bulk viscosity effects in event-by-event relativistic hydrodynamics. *Phys. Rev. C* **88**, 044916 (2013). doi:[10.1103/PhysRevC.88.044916](https://doi.org/10.1103/PhysRevC.88.044916)
127. S.A. Bass, M. Belkacem, M. Bleicher et al., Microscopic models for ultrarelativistic heavy ion collisions. *Prog. Part. Nucl. Phys.* **41**, 255–369 (1998). doi:[10.1016/S0146-6410\(98\)00058-1](https://doi.org/10.1016/S0146-6410(98)00058-1)
128. M. Bleicher, E. Zabrodin, C. Spieles, Relativistic hadron hadron collisions in the ultrarelativistic quantum molecular dynamics model. *J. Phys. G* **25**, 1859–1896 (1999). doi:[10.1088/0954-3899/25/9/308](https://doi.org/10.1088/0954-3899/25/9/308)
129. H.C. Song, S. Bass, U.W. Heinz, Spectra and elliptic flow for identified hadrons in 2.76A TeV Pb + Pb collisions. *Phys. Rev. C* **89**, 034919 (2014). doi:[10.1103/PhysRevC.89.034919](https://doi.org/10.1103/PhysRevC.89.034919)
130. U. Heinz, C. Shen, H.C. Song, The viscosity of quark–gluon plasma at RHIC and the LHC. *AIP Conf. Proc.* **1441**, 766–770 (2012). doi:[10.1063/1.3700674](https://doi.org/10.1063/1.3700674)
131. H.C. Song, QGP viscosity at RHIC and the LHC—a 2012 status report. *A904–905*, 114c–121c (2013). doi:[10.1016/j.nuclphysa.2013.01.052](https://doi.org/10.1016/j.nuclphysa.2013.01.052)
132. P. Bozek, Flow and interferometry in 3+1 dimensional viscous hydrodynamics. *Phys. Rev. C* **85**, 034901 (2012). doi:[10.1103/PhysRevC.85.034901](https://doi.org/10.1103/PhysRevC.85.034901)
133. J. Vredevoogd, S. Pratt, Viscous hydrodynamics and relativistic heavy ion collisions. *Phys. Rev. C* **85**, 044908 (2012). doi:[10.1103/PhysRevC.85.044908](https://doi.org/10.1103/PhysRevC.85.044908)
134. C. Nonaka, Y. Akamatsu, M. Takamoto, Study of higher harmonics based on (3+1)-d relativistic viscous hydrodynamics. *Nucl. Phys. A* **904–905**, 405c–408c (2013). doi:[10.1016/j.nuclphysa.2013.02.035](https://doi.org/10.1016/j.nuclphysa.2013.02.035)
135. L. Del Zanna, V. Chandra, G. Inghirami et al., Relativistic viscous hydrodynamics for heavy-ion collisions with ECHO-QGP. *Eur. Phys. J. C* **73**, 2524 (2013). doi:[10.1140/epjc/s10052-013-2524-5](https://doi.org/10.1140/epjc/s10052-013-2524-5)
136. Iu Karpenko, P. Huovinen, M. Bleicher, A 3+1 dimensional viscous hydrodynamic code for relativistic heavy ion collisions. *Comput. Phys. Commun.* **185**, 3016–3027 (2014). doi:[10.1016/j.cpc.2014.07.010](https://doi.org/10.1016/j.cpc.2014.07.010)
137. H. Petersen, G.Y. Qin, S.A. Bass et al., Triangular flow in event-by-event ideal hydrodynamics in Au+Au collisions at $\sqrt{s_{NN}} = 200$ A GeV. *Phys. Rev. C* **82**, 041901 (2010). doi:[10.1103/PhysRevC.82.041901](https://doi.org/10.1103/PhysRevC.82.041901)
138. G.Y. Qin, H. Petersen, S.A. Bass et al., Translation of collision geometry fluctuations into momentum anisotropies in relativistic heavy-ion collisions. *Phys. Rev. C* **82**, 064903 (2010). doi:[10.1103/PhysRevC.82.064903](https://doi.org/10.1103/PhysRevC.82.064903)
139. H. Holopainen, H. Niemi, K.J. Eskola, Event-by-event hydrodynamics and elliptic flow from fluctuating initial state. *Phys. Rev. C* **83**, 034901 (2011). doi:[10.1103/PhysRevC.83.034901](https://doi.org/10.1103/PhysRevC.83.034901)
140. Z. Qiu, U.W. Heinz, Event-by-event shape and flow fluctuations of relativistic heavy-ion collision fireballs. *Phys. Rev. C* **84**, 024911 (2011). doi:[10.1103/PhysRevC.84.024911](https://doi.org/10.1103/PhysRevC.84.024911)
141. C. Shen, Z. Qiu, H.C. Song et al., The iEBE-VISHNU code package for relativistic heavy-ion collisions. *Comput. Phys. Commun.* **199**, 61–85 (2016). doi:[10.1016/j.cpc.2015.08.039](https://doi.org/10.1016/j.cpc.2015.08.039)
142. D. Bazow, U.W. Heinz, M. Strickland, Massively parallel simulations of relativistic fluid dynamics on graphics processing units with CUDA (2016), [arXiv: 1608.06577](https://arxiv.org/abs/1608.06577)
143. A.M. Poskanzer, S.A. Voloshin, Methods for analyzing anisotropic flow in relativistic nuclear collisions. *Phys. Rev. C* **58**, 1671–1678 (1998). doi:[10.1103/PhysRevC.58.1671](https://doi.org/10.1103/PhysRevC.58.1671)
144. M. Luzum, J.-Y. Ollitrault, Eliminating experimental bias in anisotropic-flow measurements of high-energy nuclear collisions. *Phys. Rev. C* **87**, 044907 (2013). doi:[10.1103/PhysRevC.87.044907](https://doi.org/10.1103/PhysRevC.87.044907)
145. A. Bilandzic, R. Snellings, S. Voloshin, Flow analysis with cumulants: direct calculations. *Phys. Rev. C* **83**, 044913 (2011). doi:[10.1103/PhysRevC.83.044913](https://doi.org/10.1103/PhysRevC.83.044913)
146. A. Bilandzic, C.H. Christensen, K. Gulbrandsen et al., Generic framework for anisotropic flow analyses with multiparticle azimuthal correlations. *Phys. Rev. C* **89**, 064904 (2014). doi:[10.1103/PhysRevC.89.064904](https://doi.org/10.1103/PhysRevC.89.064904)
147. R.S. Bhalerao, M. Luzum, J.Y. Ollitrault, Determining initial-state fluctuations from flow measurements in heavy-ion collisions. *Phys. Rev. C* **84**, 034910 (2011). doi:[10.1103/PhysRevC.84.034910](https://doi.org/10.1103/PhysRevC.84.034910)
148. H.C. Song, S.A. Bass, U. Heinz et al., 200 A GeV Au+Au collisions serve a nearly perfect quark–gluon liquid. *Phys. Rev. Lett.* **106**, 192301 (2011). doi:[10.1103/PhysRevLett.106.192301](https://doi.org/10.1103/PhysRevLett.106.192301)
149. J.-Y. Ollitrault, A.M. Poskanzer, S.A. Voloshin, Effect of flow fluctuations and nonflow on elliptic flow methods. *Phys. Rev. C* **80**, 014904 (2009). doi:[10.1103/PhysRevC.80.014904](https://doi.org/10.1103/PhysRevC.80.014904)
150. B. Abelev, L. Aphecetche, G. Batigne, Elliptic flow of identified hadrons in Pb–Pb collisions at $\sqrt{s_{NN}} = 2.76$ TeV. *JHEP* **06**, 190 (2015). doi:[10.1007/JHEP06\(2015\)190](https://doi.org/10.1007/JHEP06(2015)190)
151. N. Mohammadi, Higher harmonic anisotropic flow of identified particles in Pb–Pb collisions with the ALICE detector. *Nucl. Phys. A* **956**, 304–307 (2016). doi:[10.1016/j.nuclphysa.2016.03.031](https://doi.org/10.1016/j.nuclphysa.2016.03.031)
152. H.C. Song, U.W. Heinz, Extracting the QGP viscosity from RHIC data—a status report from viscous hydrodynamics. *J. Phys. G* **36**, 064033 (2009). doi:[10.1088/0954-3899/36/6/064033](https://doi.org/10.1088/0954-3899/36/6/064033)
153. H.C. Song, S.A. Bass, U. Heinz et al., Hadron spectra and elliptic flow for 200 A GeV Au+Au collisions from viscous hydrodynamics coupled to a Boltzmann cascade. *Phys. Rev. C* **83**, 054910 (2011). doi:[10.1103/PhysRevC.83.054910](https://doi.org/10.1103/PhysRevC.83.054910)
154. H.C. Song, S.A. Bass, U. Heinz, Elliptic flow in 200 A GeV Au+Au collisions and 2.76 A TeV Pb+Pb collisions: insights from viscous hydrodynamics + hadron cascade hybrid model. *Phys. Rev. C* **83**, 054912 (2011). doi:[10.1103/PhysRevC.83.054912](https://doi.org/10.1103/PhysRevC.83.054912)
155. X.G. Zhu, F.L. Meng, H.C. Song et al., Hybrid model approach for strange and multistrange hadrons in 2.76A TeV Pb+Pb collisions. *Phys. Rev. C* **91**, 034904 (2015). doi:[10.1103/PhysRevC.91.034904](https://doi.org/10.1103/PhysRevC.91.034904)
156. J. Adam, D. Adamová, M.M. Aggarwal, Higher harmonic flow coefficients of identified hadrons in Pb–Pb collisions at $\sqrt{s_{NN}} = 2.76$ TeV. *JHEP* **09**, 164 (2016). doi:[10.1007/JHEP09\(2016\)164](https://doi.org/10.1007/JHEP09(2016)164)
157. G. Torrieri, I. Mishustin, Instability of boost-invariant hydrodynamics with a QCD inspired bulk viscosity. *Phys. Rev. C* **78**, 021901 (2008). doi:[10.1103/PhysRevC.78.021901](https://doi.org/10.1103/PhysRevC.78.021901)
158. K. Rajagopal, N. Tripuraneni, Bulk viscosity and cavitation in boost-invariant hydrodynamic expansion. *JHEP* **03**, 018 (2010). doi:[10.1007/JHEP03\(2010\)018](https://doi.org/10.1007/JHEP03(2010)018)
159. H.C. Song, U.W. Heinz, Interplay of shear and bulk viscosity in generating flow in heavy-ion collisions. *Phys. Rev. C* **81**, 024905 (2010). doi:[10.1103/PhysRevC.81.024905](https://doi.org/10.1103/PhysRevC.81.024905)

160. H.C. Song, U.W. Heinz, Viscous hydrodynamics with bulk viscosity: uncertainties from relaxation time and initial conditions. *Nucl. Phys. A* **830**, 467C–470C (2009). doi:[10.1016/j.nuclphysa.2009.10.041](https://doi.org/10.1016/j.nuclphysa.2009.10.041)
161. A. Monnai, T. Hirano, Effects of bulk viscosity at freezeout. *Phys. Rev. C* **80**, 054906 (2009). doi:[10.1103/PhysRevC.80.054906](https://doi.org/10.1103/PhysRevC.80.054906)
162. G.S. Denicol, T. Kodama, T. Koide et al., Effect of bulk viscosity on elliptic flow near QCD phase transition. *Phys. Rev. C* **80**, 064901 (2009). doi:[10.1103/PhysRevC.80.064901](https://doi.org/10.1103/PhysRevC.80.064901)
163. J. Noronha-Hostler, J. Noronha, F. Grassi, Bulk viscosity-driven suppression of shear viscosity effects on the flow harmonics at energies available at the BNL relativistic heavy ion collider. *Phys. Rev. C* **90**, 034907 (2014). doi:[10.1103/PhysRevC.90.034907](https://doi.org/10.1103/PhysRevC.90.034907)
164. S. Ryu, J.-F. Paquet, C. Shen et al., Importance of the bulk viscosity of QCD in ultrarelativistic heavy-ion collisions. *Phys. Rev. Lett.* **115**, 132301 (2015). doi:[10.1103/PhysRevLett.115.132301](https://doi.org/10.1103/PhysRevLett.115.132301)
165. R.A. Soltz, I. Garishvili, M. Cheng et al., Constraining the initial temperature and shear viscosity in a hybrid hydrodynamic model of $\sqrt{s_{NN}} = 200$ GeV Au+Au collisions using pion spectra, elliptic flow, and femtoscopic radii. *Phys. Rev. C* **87**, 044901 (2013). doi:[10.1103/PhysRevC.87.044901](https://doi.org/10.1103/PhysRevC.87.044901)
166. J.E. Bernhard, P.W. Marcy, C.F. Coleman-Smith et al., Quantifying properties of hot and dense QCD matter through systematic model-to-data comparison. *Phys. Rev. C* **91**, 054910 (2015). doi:[10.1103/PhysRevC.91.054910](https://doi.org/10.1103/PhysRevC.91.054910)
167. J.E. Bernhard, J.S. Moreland, S.A. Bass et al., Applying Bayesian parameter estimation to relativistic heavy-ion collisions: simultaneous characterization of the initial state and quark-gluon plasma medium. *Phys. Rev. C* **94**, 024907 (2016). doi:[10.1103/PhysRevC.94.024907](https://doi.org/10.1103/PhysRevC.94.024907)
168. P. Danielewicz, M. Gyulassy, Dissipative phenomena in quark gluon plasmas. *Phys. Rev. D* **31**, 53–62 (1985). doi:[10.1103/PhysRevD.31.53](https://doi.org/10.1103/PhysRevD.31.53)
169. G. Policastro, D.T. Son, A.O. Starinets, The shear viscosity of strongly coupled $N = 4$ supersymmetric Yang–Mills plasma. *Phys. Rev. Lett.* **87**, 081601 (2001). doi:[10.1103/PhysRevLett.87.081601](https://doi.org/10.1103/PhysRevLett.87.081601)
170. P. Kovtun, D.T. Son, A.O. Starinets, Viscosity in strongly interacting quantum field theories from black hole physics. *Phys. Rev. Lett.* **94**, 111601 (2005). doi:[10.1103/PhysRevLett.94.111601](https://doi.org/10.1103/PhysRevLett.94.111601)
171. B. Abelev, J. Adam, D. Adamova, Centrality dependence of π , K, p production in Pb–Pb collisions at $\sqrt{s_{NN}} = 2.76$ TeV. *Phys. Rev. C* **88**, 044910 (2013). doi:[10.1103/PhysRevC.88.044910](https://doi.org/10.1103/PhysRevC.88.044910)
172. J. Auvinen, J.E. Bernhard, S.A. Bass, Systematic extraction of QGP properties (2016), <http://inspirehep.net/record/1489219/files/arXiv:1610.00590.pdf>. arXiv: 1610.00590
173. B. Alver, G. Roland, Collision geometry fluctuations and triangular flow in heavy-ion collisions. *Phys. Rev. C* **81**, 054905 (2010). doi:[10.1103/PhysRevC.81.054905](https://doi.org/10.1103/PhysRevC.81.054905)
174. A. Adare, S. Afanasiev, C. Aidala et al., Measurements of higher-order flow harmonics in Au+Au collisions at $\sqrt{s_{NN}} = 200$ GeV. *Phys. Rev. Lett.* **107**, 252301 (2011). doi:[10.1103/PhysRevLett.107.252301](https://doi.org/10.1103/PhysRevLett.107.252301)
175. L. Adamczyk, J.K. Adkins, G. Agakishiev et al., Third harmonic flow of charged particles in Au+Au collisions at $\sqrt{s_{NN}} = 200$ GeV. *Phys. Rev. C* **88**, 014904 (2013). doi:[10.1103/PhysRevC.88.014904](https://doi.org/10.1103/PhysRevC.88.014904)
176. A. Adare, C. Aidala, N.N. Ajitanand et al., Harmonic decomposition of two-particle angular correlations in Pb–Pb collisions at $\sqrt{s_{NN}} = 2.76$ TeV. *Phys. Lett. B* **708**, 249–264 (2012). doi:[10.1016/j.physletb.2012.01.060](https://doi.org/10.1016/j.physletb.2012.01.060)
177. Y. Zhou, Searches for p_T dependent fluctuations of flow angle and magnitude in Pb–Pb and p–Pb collisions. *Nucl. Phys. A* **931**, 949–953 (2014). doi:[10.1016/j.nuclphysa.2014.08.068](https://doi.org/10.1016/j.nuclphysa.2014.08.068)
178. S.A. Voloshin, A.M. Poskanzer, A.H. Tang et al., Elliptic flow in the Gaussian model of eccentricity fluctuations. *Phys. Lett. B* **659**, 537–541 (2008). doi:[10.1016/j.physletb.2007.11.043](https://doi.org/10.1016/j.physletb.2007.11.043)
179. W. Broniowski, P. Bozek, M. Rybczynski, Fluctuating initial conditions in heavy-ion collisions from the Glauber approach. *Phys. Rev. C* **76**, 054905 (2007). doi:[10.1103/PhysRevC.76.054905](https://doi.org/10.1103/PhysRevC.76.054905)
180. L. Yan, J.Y. Ollitrault, A.M. Poskanzer, Eccentricity distributions in nucleus–nucleus collisions. *Phys. Rev. C* **90**, 024903 (2014). doi:[10.1103/PhysRevC.90.024903](https://doi.org/10.1103/PhysRevC.90.024903)
181. Y. Zhou, K. Xiao, Z. Feng et al., Anisotropic distributions in a multiphase transport model. *Phys. Rev. C* **93**, 034909 (2016). doi:[10.1103/PhysRevC.93.034909](https://doi.org/10.1103/PhysRevC.93.034909)
182. D. Teaney, L. Yan, Event-plane correlations and hydrodynamic simulations of heavy ion collisions. *Phys. Rev. C* **90**, 024902 (2014). doi:[10.1103/PhysRevC.90.024902](https://doi.org/10.1103/PhysRevC.90.024902)
183. L.G. Pang, G.Y. Qin, V. Roy et al., Longitudinal decorrelation of anisotropic flows in heavy-ion collisions at the CERN large hadron collider. *Phys. Rev. C* **91**, 044904 (2015). doi:[10.1103/PhysRevC.91.044904](https://doi.org/10.1103/PhysRevC.91.044904)
184. L.G. Pang, H. Petersen, G.Y. Qin et al., Decorrelation of anisotropic flow along the longitudinal direction. *Eur. Phys. J. A* **52**, 97 (2016). doi:[10.1140/epja/i2016-16097-x](https://doi.org/10.1140/epja/i2016-16097-x)
185. K. Xiao, L. Yi, F. Liu et al., Factorization of event-plane correlations over transverse momentum in relativistic heavy ion collisions in a multiphase transport model. *Phys. Rev. C* **94**, 024905 (2016). doi:[10.1103/PhysRevC.94.024905](https://doi.org/10.1103/PhysRevC.94.024905)
186. G.-L. Ma, Z.-W. Lin, Predictions for $\sqrt{s_{NN}} = 5.02$ TeV Pb+Pb collisions from a multi-phase transport model. *Phys. Rev. C* **93**, 054911 (2016). doi:[10.1103/PhysRevC.93.054911](https://doi.org/10.1103/PhysRevC.93.054911)
187. Y. Zhou, Review of anisotropic flow correlations in ultrarelativistic heavy-ion collisions. *Adv. High Energy Phys.* **2016**, 9365637 (2016). doi:[10.1155/2016/9365637](https://doi.org/10.1155/2016/9365637)
188. R.S. Bhalerao, J.Y. Ollitrault, S. Pal, Event-plane correlators. *Phys. Rev. C* **88**, 024909 (2013). doi:[10.1103/PhysRevC.88.024909](https://doi.org/10.1103/PhysRevC.88.024909)
189. J. Schukraft, A. Timmins, S.A. Voloshin, Ultra-relativistic nuclear collisions: event shape engineering. *Phys. Lett. B* **719**, 394–398 (2013). doi:[10.1016/j.physletb.2013.01.045](https://doi.org/10.1016/j.physletb.2013.01.045)
190. D. Teaney, L. Yan, Non linearities in the harmonic spectrum of heavy ion collisions with ideal and viscous hydrodynamics. *Phys. Rev. C* **86**, 044908 (2012). doi:[10.1103/PhysRevC.86.044908](https://doi.org/10.1103/PhysRevC.86.044908)
191. D. Teaney, L. Yan, Non-linear flow response and reaction plane correlations. *Nucl. Phys. A* **904–905**, 365c–368c (2013). doi:[10.1016/j.nuclphysa.2013.02.025](https://doi.org/10.1016/j.nuclphysa.2013.02.025)
192. R.S. Bhalerao, J.-Y. Ollitrault, S. Pal, Characterizing flow fluctuations with moments. *Phys. Lett. B* **742**, 94–98 (2015). doi:[10.1016/j.physletb.2015.01.019](https://doi.org/10.1016/j.physletb.2015.01.019)
193. L. Yan, J.Y. Ollitrault, v_4, v_5, v_6, v_7 : nonlinear hydrodynamic response versus LHC data. *Phys. Lett. B* **744**, 82–87 (2015). doi:[10.1016/j.physletb.2015.03.040](https://doi.org/10.1016/j.physletb.2015.03.040)
194. Y. Zhou (for the ALICE Collaboration), in *Quark Matter* (2017)
195. S. Tuo (for the CMS Collaboration), in *Quark Matter* (2017)
196. W. Adam, T. Bergauer, M. Dragicevic et al., Multiplicity and transverse momentum dependence of two- and four-particle correlations in pPb and PbPb collisions. *Phys. Lett. B* **724**, 213–240 (2013). doi:[10.1016/j.physletb.2013.06.028](https://doi.org/10.1016/j.physletb.2013.06.028)
197. K. Dusling, R. Venugopalan, Azimuthal collimation of long range rapidity correlations by strong color fields in high multiplicity hadron–hadron collisions. *Phys. Rev. Lett.* **108**, 262001 (2012). doi:[10.1103/PhysRevLett.108.262001](https://doi.org/10.1103/PhysRevLett.108.262001)

198. K. Dusling, R. Venugopalan, Evidence for BFKL and saturation dynamics from dihadron spectra at the LHC. *Phys. Rev. D* **87**, 051502 (2013). doi:[10.1103/PhysRevD.87.051502](https://doi.org/10.1103/PhysRevD.87.051502)
199. K. Dusling, R. Venugopalan, Explanation of systematics of CMS p+Pb high multiplicity di-hadron data at $\sqrt{s_{NN}} = 5.02$ TeV. *Phys. Rev. D* **87**, 054014 (2013). doi:[10.1103/PhysRevD.87.054014](https://doi.org/10.1103/PhysRevD.87.054014)
200. K. Dusling, R. Venugopalan, Comparison of the color glass condensate to dihadron correlations in proton–proton and proton–nucleus collisions. *Phys. Rev. D* **87**, 094034 (2013). doi:[10.1103/PhysRevD.87.094034](https://doi.org/10.1103/PhysRevD.87.094034)
201. K. Dusling, R. Venugopalan, Azimuthal anisotropy from color glass condensates in proton–nucleus collisions. *Nucl. Phys. A* **931**, 283–287 (2014). doi:[10.1016/j.nuclphysa.2014.09.024](https://doi.org/10.1016/j.nuclphysa.2014.09.024)
202. A. Kovner, M. Lublinsky, Angular and long range rapidity correlations in particle production at high energy. *Int. J. Mod. Phys. E* **22**, 1330001 (2013). doi:[10.1142/S0218301313300014](https://doi.org/10.1142/S0218301313300014)
203. A. Dumitru, A.V. Giannini, Initial state angular asymmetries in high energy p+A collisions: spontaneous breaking of rotational symmetry by a color electric field and C-odd fluctuations. *Nucl. Phys. A* **933**, 212–228 (2015). doi:[10.1016/j.nuclphysa.2014.10.037](https://doi.org/10.1016/j.nuclphysa.2014.10.037)
204. A. Dumitru, V. Skokov, Anisotropy of the semiclassical gluon field of a large nucleus at high energy. *Phys. Rev. D* **91**, 074006 (2015). doi:[10.1103/PhysRevD.91.074006](https://doi.org/10.1103/PhysRevD.91.074006)
205. J. Noronha, A. Dumitru, Azimuthal asymmetries in high-energy collisions of protons with holographic shockwaves. *Phys. Rev. D* **89**, 094008 (2014). doi:[10.1103/PhysRevD.89.094008](https://doi.org/10.1103/PhysRevD.89.094008)
206. A. Bzdak, G.L. Ma, Elliptic and triangular flow in p+Pb and peripheral Pb+Pb collisions from parton scatterings. *Phys. Rev. Lett.* **113**, 252301 (2014). doi:[10.1103/PhysRevLett.113.252301](https://doi.org/10.1103/PhysRevLett.113.252301)
207. G.L. Ma, A. Bzdak, Long-range azimuthal correlations in proton–proton and proton–nucleus collisions from the incoherent scattering of partons. *Phys. Lett. B* **739**, 209–213 (2014). doi:[10.1016/j.physletb.2014.10.066](https://doi.org/10.1016/j.physletb.2014.10.066)
208. P. Bozek, A. Bzdak, G.L. Ma, Rapidity dependence of elliptic and triangular flow in proton–nucleus collisions from collective dynamics. *Phys. Lett. B* **748**, 301–305 (2015). doi:[10.1016/j.physletb.2015.06.007](https://doi.org/10.1016/j.physletb.2015.06.007)
209. J.D. Orjuela Koop, A. Adare, D. McGlinchey et al., Azimuthal anisotropy relative to the participant plane from a multiphase transport model in central p + Au, d + Au, and $^3\text{He} + \text{Au}$ collisions at $\sqrt{s_{NN}} = 200$ GeV. *Phys. Rev. C* **92**, 054903 (2015). doi:[10.1103/PhysRevC.92.054903](https://doi.org/10.1103/PhysRevC.92.054903)
210. H.L. Li, L. He, Z.W. Lin et al., Origin of the mass splitting of azimuthal anisotropies in a multi-phase transport model (2016), [arXiv: 1604.07387](https://arxiv.org/abs/1604.07387)
211. Y. Zhou, X.R. Zhu, P.F. Li et al., Investigation of possible hadronic flow in $\sqrt{s_{NN}} = 5.02$ TeV p – Pb collisions. *Phys. Rev. C* **91**, 064908 (2015). doi:[10.1103/PhysRevC.91.064908](https://doi.org/10.1103/PhysRevC.91.064908)
212. P.M. Chesler, Colliding shock waves and hydrodynamics in small systems. *Phys. Rev. Lett.* **115**, 241602 (2015). doi:[10.1103/PhysRevLett.115.241602](https://doi.org/10.1103/PhysRevLett.115.241602)
213. P.M. Chesler, How big are the smallest drops of quark–gluon plasma? *JHEP* **03**, 146 (2016). doi:[10.1007/JHEP03\(2016\)146](https://doi.org/10.1007/JHEP03(2016)146)
214. P. Bozek, W. Broniowski, Collective dynamics in high-energy proton–nucleus collisions. *Phys. Rev. C* **88**, 014903 (2013). doi:[10.1103/PhysRevC.88.014903](https://doi.org/10.1103/PhysRevC.88.014903)
215. H. Mäntysaari, B. Schenke, Evidence of strong proton shape fluctuations from incoherent diffraction. *Phys. Rev. Lett.* **117**, 052301 (2016). doi:[10.1103/PhysRevLett.117.052301](https://doi.org/10.1103/PhysRevLett.117.052301)
216. H. Mäntysaari, B. Schenke, Revealing proton shape fluctuations with incoherent diffraction at high energy. *Phys. Rev. D* **94**, 034042 (2016). doi:[10.1103/PhysRevD.94.034042](https://doi.org/10.1103/PhysRevD.94.034042)
217. A. Adare, C. Aidala, N.N. Ajitanand et al., Quadrupole anisotropy in dihadron azimuthal correlations in central d+Au collisions at $\sqrt{s_{NN}} = 200$ GeV. *Phys. Rev. Lett.* **111**, 212301 (2013). doi:[10.1103/PhysRevLett.111.212301](https://doi.org/10.1103/PhysRevLett.111.212301)
218. A. Adare, C. Aidala, N.N. Ajitanand et al., Measurement of long-range angular correlation and quadrupole anisotropy of pions and (anti)protons in central d+Au collisions at $\sqrt{s_{NN}} = 200$ GeV. *Phys. Rev. Lett.* **114**, 192301 (2015). doi:[10.1103/PhysRevLett.114.192301](https://doi.org/10.1103/PhysRevLett.114.192301)
219. L. Adamczyk, J.K. Adkins, G. Agakishiev et al., Long-range pseudorapidity dihadron correlations in d+Au collisions at $\sqrt{s_{NN}} = 200$ GeV. *Phys. Lett. B* **747**, 265–271 (2015). doi:[10.1016/j.physletb.2015.05.075](https://doi.org/10.1016/j.physletb.2015.05.075)
220. A. Adare, S. Afanasiev, C. Aidala et al., Measurements of elliptic and triangular flow in high-multiplicity $^3\text{He} + \text{Au}$ collisions at $\sqrt{s_{NN}} = 200$ GeV. *Phys. Rev. Lett.* **115**, 142301 (2015). doi:[10.1103/PhysRevLett.115.142301](https://doi.org/10.1103/PhysRevLett.115.142301)
221. J.D. Orjuela Koop, R. Belmont, P. Yin et al., Exploring the beam energy dependence of flow-like signatures in small system d+Au collisions. *Phys. Rev. C* **93**, 044910 (2016). doi:[10.1103/PhysRevC.93.044910](https://doi.org/10.1103/PhysRevC.93.044910)
222. P. Bozek, W. Broniowski, Hydrodynamic modeling of $^3\text{He} + \text{Au}$ collisions at $\sqrt{s_{NN}} = 200$ GeV. *Phys. Lett. B* **747**, 135–138 (2015). doi:[10.1016/j.physletb.2015.05.068](https://doi.org/10.1016/j.physletb.2015.05.068)
223. P. Romatschke, Light-heavy ion collisions: a window into pre-equilibrium QCD dynamics? *Eur. Phys. J. C* **75**, 305 (2015). doi:[10.1140/epjc/s10052-015-3509-3](https://doi.org/10.1140/epjc/s10052-015-3509-3)
224. J. Adam, D. Adamov a, M.M. Aggarwal, Two-pion femtoscopy in p–Pb collisions at $\sqrt{s_{NN}} = 5.02$ TeV. *Phys. Rev. C* **91**, 034906 (2015). doi:[10.1103/PhysRevC.91.034906](https://doi.org/10.1103/PhysRevC.91.034906)
225. P. Bozek, Femtoscopy analysis of d–Au interactions at $\sqrt{s} = 200$ GeV. *Phys. Rev. C* **90**, 064913 (2014). doi:[10.1103/PhysRevC.90.064913](https://doi.org/10.1103/PhysRevC.90.064913)
226. V.M. Shapoval, P. Braun-Munzinger, Iu Karpenko, Femtoscopy scales in p + p and p+Pb collisions in view of the uncertainty principle. *Phys. Lett. B* **725**, 139–147 (2013). doi:[10.1016/j.physletb.2013.07.002](https://doi.org/10.1016/j.physletb.2013.07.002)
227. H. Niemi, G.S. Denicol, How large is the Knudsen number reached in fluid dynamical simulations of ultrarelativistic heavy ion collisions? (2014), [arXiv: 1404.7327](https://arxiv.org/abs/1404.7327)
228. B. Schenke, S. Schlichting, R. Venugopalan, Azimuthal anisotropies in p+Pb collisions from classical Yang–Mills dynamics. *Phys. Lett. B* **747**, 76–82 (2015). doi:[10.1016/j.physletb.2015.05.051](https://doi.org/10.1016/j.physletb.2015.05.051)
229. H.L. Li, L. He, Z.W. Lin et al., Origin of the mass splitting of elliptic anisotropy in a multiphase transport model. *Phys. Rev. C* **93**, 051901 (2016). doi:[10.1103/PhysRevC.93.051901](https://doi.org/10.1103/PhysRevC.93.051901)
230. H. Petersen, M. Bleicher, S.A. Bass et al., UrQMD v2.3: changes and Comparisons (2008), [arXiv: 0805.0567](https://arxiv.org/abs/0805.0567)
231. P. Romatschke, Collective flow without hydrodynamics: simulation results for relativistic ion collisions. *Eur. Phys. J. C* **75**, 429 (2015). doi:[10.1140/epjc/s10052-015-3646-8](https://doi.org/10.1140/epjc/s10052-015-3646-8)
232. A. Dumitru, K. Dusling, F. Gelis et al., The Ridge in proton–proton collisions at the LHC. *Phys. Lett. B* **697**, 21–25 (2011). doi:[10.1016/j.physletb.2011.01.024](https://doi.org/10.1016/j.physletb.2011.01.024)
233. E. Levin, A.H. Rezaeian, The Ridge from the BFKL evolution and beyond. *Phys. Rev. D* **84**, 034031 (2011). doi:[10.1103/PhysRevD.84.034031](https://doi.org/10.1103/PhysRevD.84.034031)
234. P. Tribedy, R. Venugopalan, QCD saturation at the LHC: comparisons of models to p + p and A + A data and predictions for p + Pb collisions. *Phys. Lett. B* **710**, 125–133 (2012). doi:[10.1016/j.physletb.2012.02.047](https://doi.org/10.1016/j.physletb.2012.02.047)
235. P. Bozek, Elliptic flow in proton–proton collisions at $\sqrt{s} = 7$ TeV. *Eur. Phys. J. C* **71**, 1530 (2011). doi:[10.1140/epjc/s10052-010-1530-0](https://doi.org/10.1140/epjc/s10052-010-1530-0)
236. K. Werner, Iu Karpenko, T. Pierog, The ‘Ridge’ in proton–proton scattering at 7 TeV. *Phys. Rev. Lett.* **106**, 122004 (2011). doi:[10.1103/PhysRevLett.106.122004](https://doi.org/10.1103/PhysRevLett.106.122004)

237. B. Schenke, S. Schlichting, P. Tribedy et al., Mass ordering of spectra from fragmentation of saturated gluon states in high multiplicity proton–proton collisions. *Phys. Rev. Lett.* **117**, 162301 (2016). doi:[10.1103/PhysRevLett.117.162301](https://doi.org/10.1103/PhysRevLett.117.162301)
238. A. Milov (for the ATLAS Collaboration), in *Hard Probe* (2016)
239. K. Gajdosova (for the ALICE Collaboration), in *Quark Matter* (2017)
240. M. Zhou (for the ATLAS Collaboration), in *Quark Matter* (2017)
241. J. Jia, M. Zhou, A. Trzupek, [arXiv:1701.03830](https://arxiv.org/abs/1701.03830) [nucl-th] (2017)
242. M. Guilbaud (for the CMS Collaboration), in *Quark Matter* (2017)